100-GeV large scale laser plasma electron acceleration by a multi-PW laser

Kazuhisa Nakajima (中島一久)[1,2,3*], Haiyang Lu (卢海洋)[1], Xueyan Zhao (赵学燕)[1], Baifei Shen (沈百飞)[1], Ruxin Li (李儒新)[1], and Zhizhan Xu (徐至展)[1]**

[1]*Shanghai Institute of Optics and Fine Mechanics, Chinese Academy of Sciences, Shanghai 201800, China*

[2]*High Energy Accelerator Research Organization (KEK) 1-1 Oho, Tsukuba, Ibaraki 305-0801, Japan*

[3]*Shanghai Jiao Tong University, Shanghai 200240, China*

[*]*Corresponding author: naka115@dia-net.ne.jp;* [**]*corresponding author: hylu@siom.ac.cn*

Received November 21, 2012; accepted December 7, 2012; posted online January 6, 2013

We present three possible design options of laser plasma acceleration (LPA) for reaching a 100-GeV level energy by means of a multi-petawatt laser such as the 3.5-kJ, 500-fs PETawatt Aquitane Laser (PETAL) at French Alternative Energies and Atomic Energy Commission (CEA). Based on scaling of laser wakefield acceleration in the quasi-linear regime with the normalized vector potential $a_0 = 1.4(1.6)$, acceleration to 100 (130) GeV requires a 30-m-long plasma waveguide operated at the plasma density $n_e \approx 7 \times 10^{15}$ cm^{-3} with a channel depth $\Delta n/n_e = 20\%$, while a nonlinear laser wakefield accelerator in the bubble regime with $a_0 \geqslant 2$ can reach 100 GeV approximately in a $36/a_0$-m-long plasma through self-guiding. The third option is a hybrid concept that employs a ponderomotive channel created by a long leading pulse for guiding a short trailing driving laser pulse. The detail parameters for three options are evaluated, optimizing the operating plasma density at which a given energy gain is obtained over the dephasing length and the matched conditions for propagation of relativistic laser pulses in plasma channels, including the self-guiding. For the production of high-quality beams with 1%-level energy spread and a 1π-mm-mrad-level transverse normalized emittance at 100-MeV energy, a simple scheme based on the ionization-induced injection mechanism may be conceived. We investigate electron beam dynamics and effects of synchrotron radiation due to betatron motion by solving the beam dynamics equations on energy and beam radius numerically. For the bubble regime case with $a_0 = 4$, radiative energy loss becomes 10% at the maximum energy of 90 GeV.

OCIS codes: 350.4990, 350.5400.

doi: 10.3788/COL201311.013501.

1. Introduction

In this decade, vital researches on laser-driven plasma-based acceleration (LPA) concept[1], high-energy, high-quality electron beams with energies of the GeV-level in a cm-scale plasma[2−4], qualities of a 1%-level energy spread[5], a 1π-mm-mrad-level transverse emittance[6], and a 1-fs-level bunch duration[7], ensure that the stability of reproduction is as high as that of present high-power ultra-short-pulse lasers[8,9]. These high-energy high-quality particle beams make possible a wide range of applications in fundamental researches, medical and industrial uses. For many applications of laser wakefield accelerators, stability and controllability of the beam performance such as beam energy, energy spread, emittance and charge are indispensable as well as compact and robust features of the accelerator system. In particular, there are great interests in applications for high energy physics and astrophysics that explore unprecedented high-energy frontier phenomena, for which laser plasma accelerator concepts provide us with promising tools if beam-quality issues are figured out as well as an achievable highest energy and intensity requirements.

To date, most of experimental results have been obtained from interaction of ultrashort laser pulses, $\tau_L =$ 30–80 fs with a short-scale plasma such as a few mm long gas jet and a few cm long plasma channel at the plasma density in the range of $n_e = 10^{18} - 10^{19}$ cm^{-3}, where a large amplitude plasma wave of the order of 100 GV/m is excited and traps energetic electrons to be efficiently accelerated inside a wake to high-energies of the order of 1 GeV. The leading experiments that demonstrated the production of quasi-monoenergetic electron beams[10−12] have been elucidated in terms of self-injection and successive acceleration of electrons in the nonlinear wakefield, referred to as a "bubble" that is a region where plasma electrons are blown out by radiation pressure of a laser pulse with the relativistic intensity[13,14]. The self-injection is a robust method relying on self-focusing and self-compression that occur during the propagation of relativistic laser pulses. In this mechanism, initially heated electrons with large transverse momentum are injected into nonlinear wakefields that excite betatron oscillation of accelerated electrons due to strong focusing field. Hence, suppressing the self-injection and the deterioration of beam qualities, high-quality electron beams have been produced with controlled injection schemes such as colliding optical injection[15,16], density-transition injection[17,18] and ionization-induced injection[19−21], in the quasi-linear regime of wakefields driven by a laser pulse with a moderate intensity. These injection schemes provide us with high-quality electron beam injectors for a front end of large-scale laser-plasma accelerators, aiming at acceleration up to the 100 GeV-level energy.

Recently, two-staged laser-plasma acceleration has been successfully demonstrated in combination with ionization-induced injection[22,23]. Based on recent re-

sults on vital experiments and large-scale particle-in-cell (PIC) simulations[24], the design considerations and the feasibility studies on applications for high-energy frontier collider with the TeV-class center-of-mass energy have been carried out[25,26]. Among these considerations, the most critical issue is a choice of the operating plasma density that is an underlying parameter for controlling the size, the performance and the beam dynamics. Generally speaking, from the viewpoint of the beam qualities, high energy regime is in favor of the low operating density, though such option leads to large size and high laser peak power. Furthermore, the wall-plug electric power required for running such TeV-range colliders is remarkably reduced, compared to that for high operating density[26]. The state-of-the-art of PW-class lasers allows us to study the feasibility of laser plasma accelerators toward the TeV-range in a full scale.

Since the invention of laser plasma accelerator concept[1], it has been envisaged that the advent of powerful lasers generating pulses higher than the PW-level[27] may make it possible to accelerate electron/positron beams in a compact scale to the high-energy frontier in the energy range from 100 GeV to 1 PeV[25,26,28–30], where many of questions in fundamental physics can be explored. However, although the current achievements of LPA experiments break a 1 GeV barrier in several cm-scale plasmas with the density of $10^{17}-10^{18}$ cm^{-3} driven by ∼1-PW class lasers[3,4,31], it seems to be far from reaching the high-energy frontier as long as the state-of-the-art on LPAs is simply extrapolated toward such energies. In this context, it is of practical importance to demonstrate the 100-GeV level acceleration in a full scale that is reachable up to the 130 GeV Higgs mass energy as timely drawn attention.

We consider a design of the laser plasma accelerator experiment that will be carried out at CEA (French Alternative Energies and Atomic Energy Commission) Bordeaux, where a large scale laser named PETawatt Aquitaine Laser (PETAL)[27] is capable of delivering a laser pulse with energy of > 3.5 kJ, duration of 0.5–10 picoseconds at the wavelength $\lambda_{\rm L} = 1.053$ μm. These parameters guarantee a peak power of >7 PW and a focused intensity $I > 10^{20}$ W/cm^2, i.e. the achievable normalized vector potential,

$$a_0 \equiv eA_0/m_{\rm e}c^2 \simeq 0.855\times10^{-9}I^{1/2}[{\rm W/cm^2}]\lambda_{\rm L}[\mu{\rm m}] > 9, \quad (1)$$

where A_0 is the peak amplitude of the vector potential and $m_{\rm e}c^2$ is the electron rest energy. This capability allows us to explore laser plasma acceleration operated in the entire laser wakefield regime from the linear regime to the nonlinear bubble regime.

A goal for the LPA experiment is to demonstrate laser acceleration of a high-quality electron beam with 100-GeV level energy, relative energy spread of ∼1% and normalized emittance of ∼1π mm-mrad, containing sufficiently detectable charge of the order of 100 pC (∼ 10^9 electrons) per bunch within a 30-m long neutron time-of-flight beamline outstretched from the 10-m diameter Megajoule Laser (LMJ) target chamber, which is placed in the radiation shielded area. It is conceivable that there may be several routes to reach a final goal, since it is still far from the current achievements on the LPA experiments that have shown a benchmark result of 1-GeV quasi-monoenergetic e-beam acceleration from a 3-cm gas-filled discharge capillary driven by a 40-TW, 40-fs (1.6-J) laser pulse at the plasma density $n_{\rm e} = 4.3\times10^{18}$ cm^{-3}[2] and a most recent result of highly collimated (<1-mrad divergence) e-beam acceleration beyond 2 GeV with a continuous energy spread from a 7-cm gas cell driven by a 150-J, 150-fs (1-PW) self-guided laser pulse at the plasma density $n_{\rm e} = 3.3\times10^{17}$ cm^{-3}[31]. According to the energy gain scaling on the plasma density $W \propto n_{\rm e}^{-1}$, a 100-GeV e-beam can be accelerated in the broad density range of $n_{\rm e} \sim 6.6\times10^{15} - 4.3\times10^{16}$ cm^{-3}, while the required accelerator length is roughly inferred to be $L_{\rm acc} \sim 25-30$ m from the scaling of the dephasing length $L_{\rm dp} \propto n_{\rm e}^{-3/2}$.

On the basis of a rough estimate of the operating plasma density and the accelerator size, we evaluate parameters of LPAs in this paper. The remainder of this paper is organized as follows. Section II presents an analysis of the wave equation describing the propagation of a relativistic laser pulse in plasma channels to derive the matched conditions for the laser spot radius and the group velocity. Section III presents the design of the injector relying on the ionization-induced injection mechanism and three options of laser plasma accelerators that are based on the scaling of the channel-guided LPA in the quasi-linear regime, the self-guided LPA in the bubble regime, and a hybrid concept composed of a ponderomotive-channel creator pulse followed by a LPA driving pulse, respectively. In Sec. IV, electron beam dynamics of acceleration and betatron motion is analyzed for each design case, taking into account radiation reaction force due to betatron radiation. Section V presents discussions and a summary of the design options.

2. Propagation of relativistic laser pulses in plasma channels

Consider propagation of the laser beam in a parabolic density channel of the form

$$n(r) = n_0 + \Delta n\frac{r^2}{r_0^2} = n_0 + \frac{1}{\pi r_{\rm e} r_{\rm m}^2}\frac{r^2}{r_{\rm m}^2} = n_0\left(1+\frac{r^2}{r_{\rm ch}^2}\right), \quad (2)$$

where r_0 is the laser spot radius, $r_{\rm m}$ is the matched radius, and $r_{\rm ch}$ is the channel radius at which the plasma density doubles[32,33]. These radii are related to the channel depth Δn as

$$r_{\rm m} = r_0\left(\frac{\Delta n_{\rm c}}{\Delta n}\right)^{1/4} = \left(\frac{r_{\rm ch}^2}{\pi r_{\rm e} n_0}\right)^{1/4}, \text{ and}$$
$$r_0 = r_{\rm ch}\left(\frac{\Delta n}{n_0}\right)^{1/2}, \quad (3)$$

where $\Delta n_{\rm c} = 1/(\pi r_{\rm e} r_0^2)$ is the critical channel depth. The wave equation for the normalized vector potential describing the three-dimensional evolution of a laser pulse of duration $\tau_{\rm L}$ in a fully ionized plasma can be written as[34]

$$\left(\nabla^2 - \frac{\partial^2}{c^2\partial t^2}\right)\boldsymbol{a} = k^2(1-\eta^2)\boldsymbol{a}, \quad (4)$$

where $\boldsymbol{a}$ is the normalized vector potential with the Coulomb gauge $\nabla\boldsymbol{a}=0$, $k=\omega/c$ is the free-space wavenumber along the propagation direction. The (squared) refractive index for linearly polarized electromagnetic waves in the long pulse limit ($ck_{\rm p}\tau_{\rm L}\gg 1$) is given by[32]

$$\eta^2(r,z)=1-\frac{k_{\rm p}^2}{k^2\gamma_{\rm L}}\left[1+\frac{1}{k_{\rm p}^2}\nabla_\perp^2\gamma_{\rm L}+\frac{r^2}{r_{\rm ch}^2}\right], \quad (5)$$

where $k_{\rm p}=(4\pi r_{\rm e}n_{\rm e})^{1/2}$ is the plasma wavenumber evaluated with the unperturbed on-axis density n_0 and the the classical electron radius $r_{\rm e}=e^2/mc^2$, and $\gamma_{\rm L}=(1+a^2/2)^{1/2}$ is the relativistic factor of the laser intensity for the linear polarization. In Eq. (5), the first term represents free-space propagation, and three terms in the square bracket correspond to relativistic self-focusing, ponderomotive channeling and a preformed plasma channel, respectively.

The wave Eq. (4) is simplified by changing the independent variables (z,t) into (z,ζ), where $z=z$ and $\zeta=z-\beta_{\rm g}ct$ as

$$\left[\nabla_\perp^2+2\frac{\partial^2}{\partial z\partial\zeta}+(1-\beta_{\rm g}^2)\frac{\partial^2}{\partial\zeta^2}+\frac{\partial^2}{\partial z^2}\right]\boldsymbol{a}$$
$$=\frac{k_{\rm p}^2}{\gamma_{\rm L}}\left[1+\frac{1}{k_{\rm p}^2}\nabla_\perp^2\gamma_{\rm L}+\frac{r^2}{r_{\rm ch}^2}\right]\boldsymbol{a}, \quad (6)$$

where $\beta_{\rm g}=v_{\rm g}/c$ and $v_{\rm g}$ is the linear pulse group velocity. Denoting $\boldsymbol{a}=a(r,\zeta)\exp({\rm i}k\zeta)\boldsymbol{e}_x+{\rm c.c.}$ and $k=\beta_{\rm g}\omega/c$, the wave equation becomes

$$\left[\nabla_\perp^2+2\left({\rm i}k+\frac{\partial}{\partial\zeta}\right)\frac{\partial}{\partial z}+(1-\beta_{\rm g}^2)\frac{\partial^2}{\partial\zeta^2}+\frac{\partial^2}{\partial z^2}\right]a$$
$$=k^2\left[1-\frac{1}{\beta_{\rm g}^2}+\frac{k_{\rm p}^2}{k^2\gamma_{\rm L}}\left(1+\frac{1}{k_{\rm p}^2}\nabla_\perp^2\gamma_{\rm L}+\frac{r^2}{r_{\rm ch}^2}\right)\right]a. \quad (7)$$

For a short pulse of length $c\tau_{\rm L}$ propagating in a plasma channel, the operators scale as $\nabla_\perp\sim 1/r_0$, $\partial/\partial\zeta\sim 1/c\tau_{\rm L}$, $\partial/\partial z\sim 1/Z_{\rm R}$, and $1-\beta_{\rm g}^2\sim\omega_{\rm p}^2/\omega^2+4/k^2r_0^2=\omega_{\rm p}^2/\omega^2+r_0^2/Z_{\rm R}^2$, where $Z_{\rm R}=kr_0^2/2$ is the Rayleigh length. In analysis of Eq. (7), the last term on the left hand side is neglected, provided $|\partial^2a/\partial z^2|\ll 2|\partial^2a/\partial\zeta\partial z|$, assuming $c\tau_{\rm L}\ll 2Z_{\rm R}$, and $|\partial^2a/\partial z^2|\ll(1-\beta_{\rm g}^2)|\partial^2a/\partial\zeta^2|$, assuming $(c\tau_{\rm L})^2/r_0^2\ll 1+k_{\rm p}^2r_0^2/4$[35]. Assuming the paraxial approximation and no group velocity dispersion effects, i.e., $|\partial^2a/\partial\zeta\partial z|\ll k|\partial a/\partial z|$, which implies $kc\tau_{\rm L}\gg 1$, and $(1-\beta_{\rm g}^2)|\partial^2a/\partial\zeta^2|\ll 2k|\partial a/\partial z|$, which implies $kc\tau_{\rm L}\gg(1+k_{\rm p}^2r_0^2/4)^{1/2}$, the wave equation can be reduced to

$$\left(\nabla_\perp^2+2{\rm i}k\frac{\partial}{\partial z}\right)a$$
$$=k^2\left[1-\frac{1}{\beta_{\rm g}^2}+\frac{k_{\rm p}^2}{k^2\gamma_{\rm L}}\left(1+\frac{1}{k_{\rm p}^2}\nabla_\perp^2\gamma_{\rm L}+\frac{r^2}{r_{\rm ch}^2}\right)\right]a. \quad (8)$$

The wave equation with the standard paraxial form can be solved by employing the source-dependent expansion (SDE) method[36,37], rewriting Eq. (8) in cylindrical coordinates (r,ϕ,z) as

$$\left[\frac{1}{r}\frac{\partial}{\partial r}\left(r\frac{\partial}{\partial r}\right)+\frac{1}{r^2}\frac{\partial^2}{\partial\phi^2}+2{\rm i}k\frac{\partial}{\partial z}\right]a(r,\phi,z)=S(r,\phi,z), \quad (9)$$

where $S(r,\phi,z)$ is the source function given by

$$S(r,\phi,z)=k^2\left[1-\frac{1}{\beta_{\rm g}^2}+\frac{k_{\rm p}^2}{k^2\gamma_{\rm L}}\left(1+\frac{1}{k_{\rm p}^2}\nabla_\perp^2\gamma_{\rm L}+\frac{r^2}{r_{\rm ch}^2}\right)\right]$$
$$\cdot a(r,\phi,z). \quad (10)$$

Here $a(r,\phi,z)$ is expanded with the general solution in cylindrical coordinates (r,ϕ,z) of the Laguerre-Gaussian modes as

$$a(r,\phi,z)=\sum_{\rm m}\sum_{\rm p}C_{m,p}(\phi,z)D_{\rm m}^p(r,z), \quad (11)$$

where $m=0,1,2,\cdots$, $p=0,1,2,\cdots$ are mode numbers and

$$C_{m,p}(\phi,z)=a_{\rm m}(z)\exp({\rm i}\theta_{\rm m}(z)+{\rm i}p\phi), \quad (12)$$

$$D_{\rm m}^p(r,z)=\left(\frac{2r^2}{r_{\rm s}^2(z)}\right)^{p/2}L_{\rm m}^p\left(\frac{2r^2}{r_{\rm s}^2(z)}\right)$$
$$\cdot\exp\left[-(1-{\rm i}\alpha(z))\frac{r^2}{r_{\rm s}^2(z)}\right], \quad (13)$$

and $L_{\rm m}^p(x)=(e^xx^{-p}/m!)\partial^m(e^{-x}x^{m+p})/\partial x^m$ are the generalized Laguerre polynomials, e.g. $L_0^0=1$ and $L_1^0=1-x$. Assuming that the fundamental amplitude $a_0(z)$ is dominant, i.e., $|a_0(z)|\gg|a_{m>0}(z)|$, substituting Eqs. (11)–(13) into Eqs. (9) and (10) yields the equations[32,34,38,39]

$$\frac{\partial(a_0r_{\rm s})}{\partial z}=0, \quad (14)$$

$$\alpha=\frac{kr_{\rm s}}{2}\frac{\partial r_{\rm s}}{\partial z}, \quad (15)$$

$$\frac{\partial^2r_{\rm s}}{\partial z^2}-\frac{8k_{\rm p}^2}{k^2r_{\rm s}a_0^2}\left(1-\sqrt{1+a_0^2/2}+2\ln\frac{\sqrt{1+a_0^2/2}+1}{2}\right)$$
$$-\frac{8}{k^2r_{\rm s}^3a_0^2}\ln(1+a_0^2/2)$$
$$+\frac{2k_{\rm p}^2r_{\rm s}}{k^2r_{\rm ch}^2}\left[\frac{4}{a_0^2}\left(1-\sqrt{1+a_0^2/2}+\ln\frac{\sqrt{1+a_0^2/2}+1}{2}\right)\right.$$
$$\left.+{}_4F_3(1/2,1,1,1;2,2,2;-a_0^2/2)\right]=0, \quad (16)$$

$$\frac{\partial\theta}{\partial z}=\frac{k}{2}\left(\frac{1}{\beta_{\rm g}^2}-1\right)-\frac{4\ln(1+a_0^2/2)}{kr_{\rm s}^2a_0^2}$$
$$-\frac{4k_{\rm p}^2}{ka_0^2}\ln\frac{\sqrt{1+a_0^2/2}+1}{2}$$

$$+\frac{k_{\rm p}^2 r_{\rm s}^2}{2kr_{\rm ch}^2}\left[\frac{8}{a_0^2}\left(1-\sqrt{1+a_0^2/2}+\ln\frac{\sqrt{1+a_0^2/2}+1}{2}\right)\right.$$
$$\left.+{}_4F_3(1/2,1,1,1;2,2,2;-a_0^2/2)\right], \quad (17)$$

where $a_0(z)$ is the laser amplitude, $r_{\rm s}(z)$ is the spot size, $\alpha(z)$ is the phase front curvature, $\theta(z)$ is the phase shift and ${}_{\rm p}F_q$ denotes the generalized hypergeometric series of order q and class $q-p+1$. In the limit of $a_0^2 \ll 1$, the laser spot radius Eq. (16) and the phase shift Eq. (17) become[33,35]

$$\frac{\partial^2 r_{\rm s}}{\partial z^2}=\frac{4}{k^2 r_{\rm s}^3}\left(1-\frac{r_{\rm s}^4}{r_{\rm m}^4}\right), \quad (18)$$

$$\frac{\partial\theta}{\partial z}=-\frac{2}{k}\left(\frac{1}{r_{\rm s}^2}-\frac{1}{r_{\rm m}^2}\right), \quad (19)$$

where $r_{\rm m}$ is the matched spot radius and the phase velocity is assumed to satisfy

$$\frac{\omega^2}{c^2k^2}=\frac{1}{\beta_{\rm g}^2}=1+\frac{k_{\rm p}^2}{k^2}+\frac{4}{k^2r_{\rm m}^2}, \quad (20)$$

which is the conventional dispersion relation for an electromagnetic wave with spot radius $r_{\rm m}$ in a homogeneous plasma with plasma frequency $\omega_{\rm p}$, i.e., $\omega^2=c^2k^2+\omega_{\rm p}^2+4c^2/r_{\rm m}^2$, and implies the group velocity[35]

$$\beta_{\rm g}^2=\left(\frac{1}{c}\frac{\partial\omega}{\partial k}\right)^2=\frac{c^2k^2}{\omega^2}=(1+\frac{k_{\rm p}^2}{k^2}+\frac{4}{k^2r_{\rm m}^2})^{-1}$$
$$\approx 1-\frac{k_{\rm p}^2}{k^2}-\frac{4}{k^2r_{\rm m}^2}. \quad (21)$$

The spot radius and phase Eqs. (18) and (19) indicate that no variation of the spot size and the phase occur for the matched condition, i.e., $r_{\rm s}=r_{\rm m}=r_0$.

Using $X=r_{\rm s}/\widehat{a}\widehat{r}$ and $a_0=X^{-1}$, where $\widehat{a}$ and $\widehat{r}$ are the vacuum amplitude and the minimum spot size at focus, respectively, the equation for the laser beam envelope is written as[32,34,38,39]

$$\frac{\partial^2 X}{\partial z^2}+\frac{1}{\widehat{a}^4 Z_{\rm R}^2}\frac{\partial V}{\partial X}=0, \quad (22)$$

where V is defined by

$$\frac{\partial V}{\partial X}=-64\frac{P}{P_{\rm c}}X\left(1-\sqrt{1+X^{-2}/2}\right.$$
$$\left.+2\ln\frac{\sqrt{1+X^{-2}/2}+1}{2}\right)-\frac{2\ln(1+X^{-2}/2)}{X}+2N_{\rm ch}X$$
$$\cdot\left[4X^2\left(1-\sqrt{1+X^{-2}/2}+\ln\frac{\sqrt{1+X^{-2}/2}+1}{2}\right)\right.$$
$$\left.+{}_4F_3(1/2,1,1,1;2,2,2;-X^{-2}/2)\right], \quad (23)$$

and $Z_{\rm R}=k\widehat{r}^2/2$ is the Rayleigh length in vacuum, and $P/P_{\rm c}=k_{\rm p}^2\widehat{a}^2\widehat{r}^2/32$ is the ratio of the laser beam power to the critical power for the relativistic self-focusing at the plasma density n_0, given by $P_{\rm c}=17n_{\rm c}/n_0({\rm GW})$, and

$$N_{\rm ch}=\left(\frac{16}{k_{\rm p}r_{\rm ch}}\frac{P}{P_{\rm c}}\right)^2 \quad (24)$$

is a dimensionless focusing strength parameter that indicates both relativistic and channel focusing. Equation (22) represents the motion of a "particle" represented by X, in an effective potential $V(X,P/P_{\rm c},N_{\rm ch})$ and can be integrated as

$$\frac{1}{2}\left(\frac{{\rm d}X}{{\rm d}z}\right)^2+\frac{1}{\widehat{a}^4Z_{\rm R}^2}V={\rm const.} \quad (25)$$

The phase Eq. (17) is rewritten as[32]

$$\frac{\partial\theta}{\partial z}=\frac{k}{2}\left(\frac{1}{\beta_{\rm g}^2}-1\right)-\frac{1}{\widehat{a}^2Z_{\rm R}}\left\{64\frac{P}{P_{\rm c}}X^2\ln\frac{\sqrt{1+X^{-2}/2}+1}{2}\right.$$
$$+2\ln(1+X^{-2}/2)-N_{\rm ch}X^2$$
$$\cdot\left[8X^2\left(1-\sqrt{1+X^{-2}/2}+\ln\frac{\sqrt{1+X^{-2}/2}+1}{2}\right)\right.$$
$$\left.\left.+{}_4F_3(1/2,1,1,1;2,2,2;-X^{-2}/2)\right]\right\}. \quad (26)$$

Equations (22) and (26) describes the evolution of the scaled spot radius $X(z)=r_{\rm s}(z)/\widehat{a}\widehat{r}$ and the phase $\theta\,(z)$ with the initial conditions $r_{\rm s}=r_{\rm i}$, $(\partial r_s/\partial z)_i$, and $\theta_{\rm i}$ at $z=0$. The matched condition for the beam propagating with a constant spot size, i.e., the equilibrium solution $r_{\rm s}=r_0=\widehat{r}$ is derived from $\partial V/\partial X=0$ at $X=1/a_0$ in Eq. (23). The matched spot radius $r_{\rm m}=r_0$ is given by

$$k_{\rm p}^2r_{\rm m}^2=\ln(1+a_0^2/2)$$
$$\times\left\{\sqrt{1+a_0^2/2}-1-2\ln\frac{\sqrt{1+a_0^2/2}+1}{2}\right.$$
$$+\frac{\Delta n}{n_0}\left[1-\sqrt{1+a_0^2/2}+\ln\frac{\sqrt{1+a_0^2/2}+1}{2}\right.$$
$$\left.\left.+\frac{a_0^2}{4}{}_4F_3(1/2,1,1,1;2,2,2;-a_0^2/2)\right]\right\}^{-1}, \quad (27)$$

and the matched power $P_{\rm m}$ is

$$P_{\rm m}=\frac{k_{\rm p}^2r_{\rm m}^2a_0^2}{32}P_{\rm c}, \quad (28)$$

where $r_0^2/r_{\rm ch}^2=\Delta n/n_0$ is used. For the matched condition, the phase velocity is derived from $\partial\theta/\partial z=0$ at $X=1/a_0$ in Eq. (26) as

$$\frac{\omega^2}{c^2k^2}=\frac{1}{\beta_{\rm g}^2}$$
$$=1+\frac{k_{\rm p}^2}{k^2}\left[\frac{8}{a_0^2}\left(\sqrt{1+a_0^2/2}-1-\ln\frac{\sqrt{1+a_0^2/2}+1}{2}\right)\right.$$
$$\left.+\frac{\Delta n}{n_0}{}_4F_3(1/2,1,1,1;2,2,2;-a_0^2/2)\right]. \quad (29)$$

In the limit of $a_0^2 \ll 1$, Eq. (29) becomes Eq. (20). Hence, the group velocity leads to

$$\beta_{\rm g}^2 = \frac{c^2k^2}{\omega^2} \approx 1 - \frac{k_{\rm p}^2}{\kappa_{\rm ch}k^2}, \tag{30}$$

where a reduction factor of the group velocity is defined as

$$\kappa_{\rm ch}(a_0^2, \Delta n/n_0) = \frac{a_0^2}{8}\left[\left(\sqrt{1+a_0^2/2} - 1 - \ln\frac{\sqrt{1+a_0^2/2}+1}{2}\right) + \frac{\Delta n}{n_0}\frac{a_0^2}{8}{}_4F_3(1/2,1,1,1;2,2,2;-a_0^2/2)\right]^{-1}. \tag{31}$$

For the matched condition due to the self-guiding and the ponderomotive channeling, the spot radius and the group velocity are given by Eqs. (27) and (30), respectively, where the channel depth is set to $\Delta n = 0$. Figure 1 shows the dimensionless matched spot radius $k_{\rm p}r_{\rm m}$ and the reduction factor of the group velocity $\kappa_{\rm ch}$ as a function of a_0 for the normalized channel depth $\Delta n/n_0$, including the self-guiding $\Delta n/n_0 = 0$.

3. Design of large scale laser plasma accelerators

A laser plasma accelerator is composed of a gas jet or a short gas cell (injector) followed by a long uniform low-density plasma or preformed plasma channel (accelerator).

3.1 Injectors employing the ionization-induced injection

To date, successfully demonstrated are several injection schemes[8−18] that produce high-quality electron beams with small energy spread, low transverse emittance and high stability. For a large scale LPA experiment, e-beams may be produced and accelerated in the injector stage by the same driving laser pulse as that in the accelerator stage, relying on the robust self-injection mechanism. Here we consider the ionization-induced injection scheme[19−22,40].

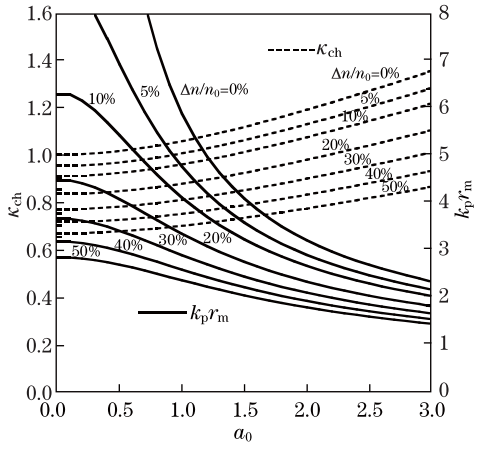

Fig. 1. The dimensionless matched spot radius $k_{\rm p}r_{\rm m}$ and the reduction factor of the group velocity $\kappa_{\rm ch}$ as a function of a_0 for the normalized channel depth $\Delta n/n_0$, including the self-guiding case $\Delta n/n_0 = 0$.

A mechanism of the ionization-induced trapping is elucidated by the fact that likely trapped are a number of electrons that are produced from impurity of gas with a large difference of the ionization potential between the outer shell electrons and the inner shell ones such as Nitrogen, of which two K-shell electrons are ionized by the optical field ionization over the barrier suppression ionization (BSZ) threshold

$$I_{\rm BSI} = \frac{cU_{\rm i}^4}{128\pi e^6Z^2} \approx \frac{2.2\times10^{15}}{Z^2}\left(\frac{U_{\rm i}}{27.21}\right)^4 ({\rm W/cm^2}) \approx 1.04\times10^{19}(1.62\times10^{19})\ {\rm W/cm^2}, \tag{32}$$

for the Nitrogen ionization state N^{6+} (N^{7+}), where Z is the charge state and the ionization potential $U_{\rm i}$ = 552.057(667.029) eV, corresponding to $a_{\rm th} \approx 2.9(3.6)$, whereas the outer shell electrons up to N^{5+} are ionized below the intensity of $I_{\rm BS} \simeq 1.47\times10^{16}(9\times10^{15})$ W/cm^2 for the N^{5+} (N^{4+}) ionization potential of 97.888 (77.472) eV and can be considered pre-ionized in the leading front of the laser pulse before the bubble formation. Hence the inner shell electrons are produced only near the peak intensity of the laser pulse, which is located near the bubble center on the propagation axis, where the wake potential is a maximum and the expelling ponderomotive force of the laser pulse is a minimum. Contrary to pre-ionized free electrons, whose trajectories move along a narrow sheath with radius $R_{\rm B}$ outside the bubble, the ionized electrons emitted from the inner shell move close to the bubble axis toward the back of the bubble where the wake potential is a minimum, and eventually trapped into the wakefield when electrons gain a sufficient kinetic energy required for trapping. This mechanism occurs at the intensity as low as the optical field ionization threshold for the inner shell electrons of impurity gas and significantly increases the trapped charge. As trapping occurs close to the bubble axis, amplitudes of the betatron oscillation after trapping decrease compared to the self-injection from the electron sheath. Recent experiments[19−22] support the ionization-induced trapping mechanism that reduces the self-injection threshold to $P/P_{\rm c} \sim 1.4$ ($a_{\rm th} \sim 1.6$) for 9:1 He:N_2 gas mixture of $n_{\rm e} \sim 1.4\times10^{19}$ cm^{-3}, increases 4∼5 times the charge for 1.2% N_2 98.8% He gas mixture of $n_{\rm e} \sim 2\times10^{19}$ cm^{-3} with the 30-TW, 30-fs laser pulse, and produces significantly collimated electron beams.

According to theoretical considerations on the ionization-induced injection[40], for trapping electrons ionized at the peak of the laser electric field, the minimum laser intensity is given by

$$1 - \gamma_{\rm p}^{-1} \leqslant 0.64a_{\rm min}^2, \tag{33}$$

where $\gamma_{\rm p} = (n_{\rm c}/n_{\rm e})^{1/2}$ is the Lorentz factor corresponding to the plasma-wave phase velocity $\beta_{\rm p} = (1 - \omega_{\rm p}^2/\omega^2)^{1/2}$. For the quasi-linear laser wakefield at $n_{\rm e} \approx 7\times10^{15}$ cm^{-3}, the required minimum laser field is $a_{\rm min} \geqslant 1.25$. The maximum number of trapped electrons is saturated to be approximately $N_{\rm e\,max} \sim 5\times10^6$ μm^{-2} at the mixed gas length $L_{\rm mix} \approx 1\,000\lambda_{\rm L}$ for the plasma density

$n_e = 0.001 n_c$ with the nitrogen concentration of $\alpha_N = 1\%$ and the laser parameters $a_0 = 2$ and $c\tau_L \approx 15\lambda_L$ due to the beam loading effects and initially trapped particle loss from the separatrix in the phase space. From the PIC-simulation results[40], the number of trapped electrons scales as

$$N_e(\mu m^{-2}) \sim 8 \times 10^7 \alpha_N k_p L_{mix} (n_e/n_c)^{1/2}, \quad (34)$$

for $\alpha_N k_p L_{mix} \leqslant 2$. The energy spread is also proportional to both the mixed gas length and the nitrogen concentration. For the quasi-linear laser wakefield case, setting $\alpha_N \approx 2\%$ and $L_{mix} \approx 15.7/k_p \approx 1$ mm, the number of electrons trapped inside the bunch with radius $r_b = 1/k_p \approx 64$ μm is estimated as

$$N_b \sim \frac{k_p^2 r_b^2}{4 r_e n_e} N_e \approx 7.1 \times 10^6 \alpha_N k_p L_{mix} k_p^2 r_b^2 \left(\frac{n_c}{n_e}\right)^{1/2} \cdot \left(\frac{\lambda_L}{1.053\ \mu m}\right)^2 \approx 8.4 \times 10^8, \quad (35)$$

which corresponds to the charge of $Q_b \sim 135$ pC. This injector can produce the high-quality beam with the relative energy spread of less than 1%. According to the 2D-PIC simulation for $a_0 = 2$[40], the energy spread of a trapped electron beam may scale as $\delta E/E = 0.2(\%)(L_{mix}/\lambda_L)(n_e/10^{15}\ \mathrm{cm}^{-3})^{-1/2}$, while the transverse normalized emittance is estimated to be $\varepsilon_{n0} \approx 5\ (\mu m) a_0^{1/2} (n_e/10^{15}\ \mathrm{cm}^{-3})^{-1/2}$.

Technically a gas jet with nozzle width of 1 mm is attached at the upstream position from the entrance of the accelerator plasma, taking into account matching of the laser pulse to the plasma channel. In the gas jet, the hydrogen gas density is set to be $n_H = (1-\alpha_N) n_e/(1+4\alpha_N) = 0.91 n_e$ and the nitrogen gas density $n_N = \alpha_N n_H/(1-\alpha_N) = \alpha_N n_e/(1+4\alpha_N) = 0.0185 n_e$ for $\alpha_N = 0.02$.

3.2 Laser plasma accelerators in the quasi-linear regime

In the linear laser wakefield with the accelerating field $E_z = E_{z0} \cos \Psi$, equations of the longitudinal motion of an electron with the normalized velocity $\beta_z = v_z/c \approx 1$ and energy $\gamma = E/m_e c^2$ are given by[41]

$$\frac{d\gamma}{dz} = k_p \frac{E_{z0}}{E_0} \cos \Psi, \quad (36)$$

$$\frac{d\Psi}{dz} = k_p \left(1 - \frac{\beta_p}{\beta_z}\right) \approx k_p (1 - \beta_g) \approx \frac{k_p}{2\gamma_b^2}, \quad (37)$$

where $\Psi = k_p(z - v_p t) + \Psi_0$ is a phase of the plasma wave, $E_0 = mc\omega_p/e$ is the nonrelativistic wave-breaking field approximately given by $E_0 \approx 96(\mathrm{GV/m})(n_e/10^{18}(\mathrm{cm}^{-3}))^{1/2}$, $\beta_p = v_p/c \approx v_g/c = \beta_g$ is the phase velocity v_p of the plasma wave normalized to c, and $\gamma_g = (1-\beta_g^2)^{-1/2} \gg 1$ is assumed. Integrating Eqs. (36) and (37), the energy and phase of the electron can be calculated as

$$\gamma(z) = \gamma_0 + 2\gamma_g^2 \frac{E_{z0}}{E_0} [\sin \Psi(z) - \sin \Psi_0] \text{ and } \Psi(z) \approx \frac{k_p z}{2\gamma_g^2} + \Psi_0. \quad (38)$$

Setting the initial electron phase $\Psi_0 = 0$ at $z = 0$, the maximum energy gain is given by

$$\Delta\gamma_{max} = \gamma_{max} - \gamma_0 = 2\gamma_g^2 \frac{E_{z0}}{E_0}, \quad (39)$$

at $k_p z = \pi\gamma_g^2$ or $z = \lambda_p \gamma_g^2/2$. As shown from Eq. (38), setting $\Psi_0 = -\pi/2$, the maximum energy gain reaches $\Delta\gamma_{max} = 4\gamma_g^2 E_{z0}/E_0$ at $k_p z = 2\pi\gamma_g^2$ or $z = \lambda_p \gamma_g^2$. However, electrons undergo both acceleration and focusing only for $0 \leqslant \Psi \leqslant \pi/2$. Hence, we define the dephasing length as $L_{dp} = \lambda_p \gamma_g^2/2$. Considering a driving laser pulse of the normalized intensity a_0^2 moving in a plasma channel with the channel depth Δn at the group velocity $\beta_g = v_g/c$ given by Eq. (30) with the corresponding relativistic factor of

$$\gamma_g^2 = \frac{1}{1-\beta_g^2} \approx \kappa_{ch} \frac{k^2}{k_p^2} = \kappa_{ch} \frac{\omega^2}{\omega_p^2} = \kappa_{ch} \frac{n_c}{n_e} = \kappa_{ch} \gamma_{g0}^2, \quad (40)$$

where $\gamma_{g0} = \omega/\omega_p$ is the relativistic factor for the group velocity in a uniform plasma and its reduction factor κ_{ch} is given by Eq. (31), the maximum energy gain and the dephasing length are written as $\Delta\gamma_{max} = 2\kappa_{ch}\gamma_{g0}^2 (E_{z0}/E_0)$ and $L_{dp} = (\lambda_p/2)\kappa_{ch}\gamma_{go}^2$, respectively. In the limit of $a_0^2 \ll 1$, $\kappa_{ch} \approx (1 + \Delta n/n_0)^{-1}$.

In the quasi-linear regime, neglecting the beam loading, the maximum accelerating field is given by[26]

$$\frac{E_{z0}}{E_0} \simeq \sqrt{\pi} a_0^2 \left(\frac{k_p \sigma_L}{4}\right) \exp\left(-\frac{k_p^2 \sigma_L^2}{4}\right) \approx 0.38 a_0^2, \quad (41)$$

for a driving laser pulse with a Gaussian temporal profile with the full-width at half-maximum (FWHM) length $c\tau_L \sim 0.375\lambda_p$, i.e., $k_p \sigma_L = \sqrt{2}$, where σ_L is the rms pulse length. For a given laser pulse duration τ_L, the operating plasma density is given by

$$n_e = \frac{2}{k^2 \sigma_L^2} n_c = \frac{2\ln 2}{\pi^2} \left(\frac{\lambda_L}{c\tau_L}\right)^2 n_c \approx 7 \times 10^{15} (\mathrm{cm}^{-3}) \left(\frac{500\ \mathrm{fs}}{\tau_L}\right)^2, \quad (42)$$

where $k = 2\pi/\lambda_L$ is the laser wave number. At this plasma density, the energy gain is written as

$$\Delta\gamma_{max} = \frac{W_{max}}{m_e c^2} = 2\kappa_{ch}\gamma_{g0}^2 \frac{E_{z0}}{E_0} \approx 0.76 \kappa_{ch} a_0^2 \frac{n_c}{n_e} = 1.09 \times 10^5 \kappa_{ch} a_0^2 \left(\frac{\tau_L}{500\ \mathrm{fs}}\right)^2. \quad (43)$$

The normalized laser intensity a_0^2 is restricted by the condition that the dephasing length is shorter than the pump depletion length, i.e., for $k_p \sigma_L = \sqrt{2}$,

$$k_p L_{dp} = \pi \kappa_{ch} \frac{n_c}{n_e} \leqslant k_p L_{pd} \simeq \frac{8.7}{a_0^2} \frac{n_c}{n_e}, \quad (44)$$

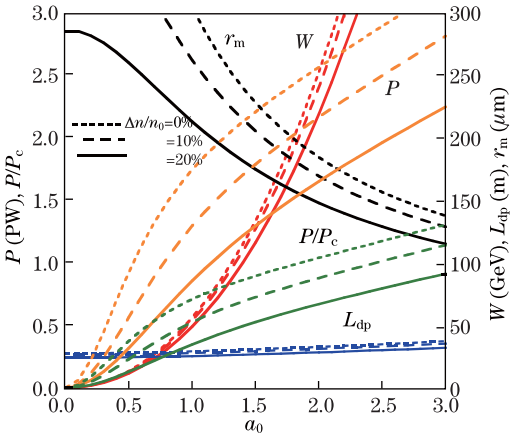

Fig. 2. For the quasi-linear regime LPA, parameters of energy gain W(GeV), dephasing length L_{dp}(m), matched spot radius $r_m(\mu m)$, matched peak power P(PW), and the ratio of the peak power to the relativistic self-focusing critical power P/P_c for the operating plasma density $n_e = 7\times10^{15}$ cm^{-3} and the channel depth $\Delta n/n_e = 5, 10, 20\%$ as a function of the normalized vector potential a_0.

where L_{pd} is the pump depletion length, at which the total field energy becomes equal to half the initial laser energy. In the limit of $a_0^2 \ll 1$, this condition leads to $a_0 \leqslant 1.66(1+\Delta n/n_0)^{1/2}$. Thus, the required accelerator length L_{acc} can be set to be

$$L_{acc} = L_{dp} = \kappa_{ch}\frac{\lambda_p}{2}\frac{n_c}{n_e} = \frac{\pi^3\lambda_L\kappa_{ch}}{4\sqrt{2}(\ln 2)^{3/2}}\left(\frac{c\tau_L}{\lambda_L}\right)^3$$
$$\approx 28.9(\mathrm{m})\kappa_{ch}\left(\frac{1.053\ \mu\mathrm{m}}{\lambda_L}\right)^2\left(\frac{\tau_L}{500\ \mathrm{fs}}\right)^3, \quad (45)$$

where n_c/n_e is given by Eq. (42).

Parameters of energy gain W(GeV), dephasing length L_{dp}(m), matched spot radius $r_m(\mu m)$, matched peak power P(PW), and the ratio of the peak power to the self- focusing critical power P/P_c are shown for the operating plasma density $n_e = 7\times10^{15}$ cm^{-3} and the channel depth $\Delta n/n_e = 5, 10, 20\%$ in Fig. 2 as a function of the normalized vector potential a_0.

3.3 Laser plasma accelerators in the bubble regime

In the bubble (blowout) regime[13,14] for $a_0 \geqslant 2$, since an electron-evacuated cavity shape is determined by balancing the Lorentz force of the ion sphere exerted on the electron sheath with the ponderomotive force of the laser pulse, the bubble radius R_B is approximately given as[14]

$$k_p R_B \approx 2\sqrt{a_0}. \quad (46)$$

The maximum accelerating field is given by

$$\frac{E_{z0}}{E_0} = \frac{1}{2}\alpha k_p R_B, \quad (47)$$

where $\alpha \approx 0.9$ represents a factor taking into account the difference between the simulation and theoretical estimation.

1) Self-guided case

The equations of longitudinal motion of an electron are approximately written as

$$\frac{d\gamma}{dz} = k_p\frac{E_{z0}}{E_0}(R_B - \xi) = \frac{1}{2}\alpha k_p^2 R_B\left(1 - \frac{\xi}{R_B}\right), \quad (48)$$

$$\frac{d\xi}{dz} = 1 - \frac{\beta_B}{\beta_z} \approx 1 - \beta_B \approx \frac{3}{2\gamma_g^2}, \quad (49)$$

where $\xi = z - v_B t$ $(0 \leqslant \xi \leqslant R_B)$ is the longitudinal coordinate of the bubble frame moving at the velocity of $v_B = c\beta_B \approx v_g - v_{etch}$ and taking into account the diffraction at the laser front that etches back at the velocity of $v_{etch} \sim c(\omega_p/\omega)^2$[42]. Integrating the Eqs. (48) and (49), the energy and phase of the electron can be calculated as

$$\gamma(z) = \gamma_0 + \frac{1}{3}\alpha\gamma_g^2 k_p^2 R_B\xi(z)\left(1 - \frac{\xi(z)}{2R_B}\right), \text{ and}$$
$$\xi(z) = \frac{3z}{2\gamma_g^2}, \quad (50)$$

where $\gamma_0 = \gamma(0)$ is the injection energy. Hence, the maximum energy gain is obtained from

$$\Delta\gamma_{max} = \gamma_{max} - \gamma_0 \approx \frac{1}{6}\alpha\gamma_g^2 k_p^2 R_B^2 \approx \frac{2}{3}\alpha a_0\gamma_g^2$$
$$= \frac{2}{3}\alpha\kappa_{self}a_0\frac{n_c}{n_e}, \quad (51)$$

at $\zeta = R_B$, i.e., the dephasing length L_{dp} for self-guided bubble regime is

$$k_p L_{dp} \approx \frac{2}{3}k_p R_B\gamma_g^2 = \frac{4}{3}\sqrt{a_0}\kappa_{self}\frac{n_c}{n_e}, \quad (52)$$

where κ_{self} is given by

$$\kappa_{self} \equiv \kappa_{ch}(a_0^2, 0)$$
$$= \frac{a_0^2}{8}\left(\sqrt{1+a_0^2/2} - 1 - \ln\frac{\sqrt{1+a_0^2/2}+1}{2}\right)^{-1}. \quad (53)$$

The operating plasma density is determined from Eq. (51) as

$$n_e = \frac{2}{3}\alpha\kappa_{self}a_0\frac{n_c}{\Delta\gamma_{max}} \approx 3.4\times10^{15}(\mathrm{cm}^{-3})\kappa_{self}a_0$$
$$\cdot\left(\frac{1.053\ \mu\mathrm{m}}{\lambda_L}\right)^2\left(\frac{100\ \mathrm{GeV}}{W/\alpha}\right), \quad (54)$$

and the accelerator length becomes

$$L_{acc} = L_{dp} \approx \sqrt{\frac{3}{2}}\frac{(\Delta\gamma_{max}/\alpha)^{3/2}}{\pi\kappa_{self}^{1/2}a_0}\lambda_L$$
$$\approx \frac{36(\mathrm{m})}{\kappa_{self}^{1/2}a_0}\left(\frac{\lambda_L}{1.053\ \mu\mathrm{m}}\right)\left(\frac{W/\alpha}{100\ \mathrm{GeV}}\right)^{3/2}. \quad (55)$$

The dephasing length should be less than the pump depletion length due to pulse-front erosion $L_{pd} \sim$

$c\tau_{\rm L} n_{\rm c}/n_{\rm e} \geqslant L_{\rm dp}$. Therefore, the pulse length is set to be

$$c\tau_{\rm L} \geqslant \frac{2}{3\pi}\sqrt{a_0}\kappa_{\rm self}\lambda_{\rm p}, \text{ or}$$
$$k_{\rm p}\sigma_{\rm L} \geqslant \frac{2}{3}\kappa_{\rm self}\left(\frac{a_0}{\ln 2}\right)^{1/2} \approx 0.8\kappa_{\rm self}\sqrt{a_0}. \quad (56)$$

This condition restricts the operating plasma density to

$$n_{\rm e} \geqslant \left(\frac{2\kappa_{\rm self}\lambda_{\rm L}}{3\pi c\tau_{\rm L}}\right)^2 a_0 n_{\rm c}$$
$$\approx 2.23\times 10^{15}({\rm cm}^{-3}) a_0 \kappa_{\rm self}^2 \left(\frac{500\ {\rm fs}}{\tau_{\rm L}}\right)^2. \quad (57)$$

Equations (54) and (57) suggest that the pulse duration satisfies

$$\tau_{\rm L} \geqslant 405({\rm fs})\kappa_{\rm self}^{1/2}\left(\frac{\lambda_{\rm L}}{1.053\ \mu{\rm m}}\right)\left(\frac{W/\alpha}{100\ {\rm GeV}}\right)^{1/2}. \quad (58)$$

for self-guiding a driving laser pulse.

For energy gain $W = 100$ GeV and $\alpha = 0.9$, Figure 3 shows parameters of operating plasma density $n_{\rm e}(10^{15}\ {\rm cm}^{-3})$, dephasing length $L_{\rm dp}({\rm m})$, pump depletion length $L_{\rm pd}({\rm m})$, matched spot radius $r_{\rm m}(\mu{\rm m})$, matched peak power $P({\rm PW})$, and the ratio of the peak power to the relativistic self-focusing critical power $P/P_{\rm c}$ along with the dimensionless matched radius $R_{\rm m} = k_{\rm p} r_{\rm m}$ and the group velocity factor $\kappa_{\rm self}$ as a function of the normalized vector potential a_0.

2) Channel-guided case

For a driving laser pulse propagating in a plasma channel, the equations of an electron motion are given by setting $v_{\rm B} = c\beta_{\rm B} \approx v_{\rm g}$ in Eq. (49), i.e., ${\rm d}\zeta/{\rm d}z \approx 1 - \beta_{\rm B} \approx 1/2\gamma_{\rm g}^2$. Hence, the maximum energy gain results in

$$\Delta\gamma_{\rm max} = \gamma_{\rm max} - \gamma_0 \approx \frac{1}{2}\alpha\gamma_{\rm g}^2 k_{\rm p}^2 R_{\rm B}^2 \approx 2\alpha a_0 \gamma_{\rm g}^2$$
$$= 2\alpha\kappa_{\rm ch} a_0 \frac{n_{\rm c}}{n_{\rm e}}, \quad (59)$$

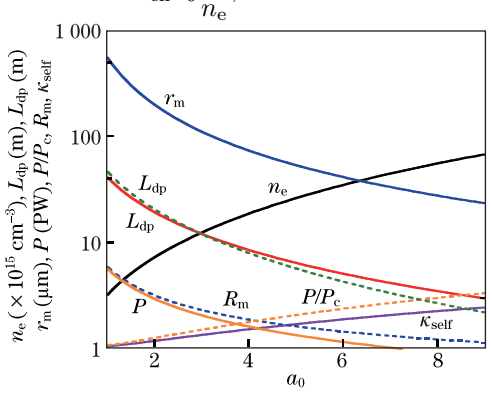

Fig. 3. For the self-guiding LPA with energy gain $W = 100$ GeV and $\alpha = 0.9$, parameters of operating plasma density $n_{\rm e}(\times 10^{15}\ {\rm cm}^{-3})$, dephasing length $L_{\rm dp}({\rm m})$, pump depletion length $L_{\rm pd}({\rm m})$, matched spot radius $r_{\rm m}(\mu{\rm m})$, matched peak power $P({\rm PW})$, and the ratio of the peak power to the relativistic self-focusing critical power $P/P_{\rm c}$ along with the dimensionless matched radius $R_{\rm m} = k_{\rm p} r_{\rm m}$ and the group velocity factor $\kappa_{\rm self}$ as a function of the normalized vector potential a_0.

and the dephasing length is

$$k_{\rm p} L_{\rm dp} \approx 2k_{\rm p} R_{\rm B} \gamma_{\rm g}^2 = 4\sqrt{a_0}\kappa_{\rm ch}\frac{n_{\rm c}}{n_{\rm e}}, \quad (60)$$

where $\kappa_{\rm ch}$ is given by Eq. (31). The operating plasma density is determined by

$$n_{\rm e} = 2\alpha\kappa_{\rm ch} a_0 \frac{n_{\rm c}}{\Delta\gamma_{\rm max}} \approx 1.03\times 10^{16}({\rm cm}^{-3})\kappa_{\rm ch} a_0$$
$$\cdot \left(\frac{1.053\ \mu{\rm m}}{\lambda_{\rm L}}\right)^2 \left(\frac{100\ {\rm GeV}}{W/\alpha}\right), \quad (61)$$

and the accelerator length becomes

$$L_{\rm acc} = L_{\rm dp} \approx \frac{\lambda_{\rm L}}{\sqrt{2}\pi\kappa_{\rm ch}^{1/2} a_0}\left(\frac{\Delta\gamma_{\rm max}}{\alpha}\right)^{3/2}$$
$$\approx \frac{20.5({\rm m})}{\kappa_{\rm ch}^{1/2} a_0}\left(\frac{\lambda_{\rm L}}{1.053\ \mu{\rm m}}\right)\left(\frac{W/\alpha}{100\ {\rm GeV}}\right)^{3/2}. \quad (62)$$

The pump depletion length, at which the total field energy becomes half of the initial laser energy, is given by

$$L_{\rm pd} \approx \frac{\sqrt{\pi}}{2\alpha^2} a_0 \sigma_{\rm L}\frac{n_{\rm c}}{n_{\rm e}} \approx \frac{0.53}{\alpha^2} a_0 c\tau_{\rm L}\frac{n_{\rm c}}{n_{\rm e}}$$
$$\approx \frac{7.8({\rm m})}{\alpha^2\kappa_{\rm ch}}\left(\frac{W/\alpha}{100\ {\rm GeV}}\right)\left(\frac{\tau_{\rm L}}{500\ {\rm fs}}\right). \quad (63)$$

The requirement for the accelerator length $L_{\rm acc} = L_{\rm dp} \leqslant L_{\rm pd}$ bounds the minimum pulse duration

$$\tau_{\rm L} \geqslant 1.3({\rm ps})\frac{\alpha^2\kappa_{\rm ch}^{1/2}}{a_0}\left(\frac{\lambda_{\rm L}}{1.053\ \mu{\rm m}}\right)\left(\frac{W/\alpha}{100\ {\rm GeV}}\right)^{1/2}. \quad (64)$$

3.4 Ponderomotive channel-guided laser plasma accelerators

The radial ponderomotive force of a long laser pulse ($c\tau_{\rm G} > \lambda_{\rm p}$) propagating in an initially uniform plasma can expel electrons from the axis, thus creating a density channel, of which the relative density perturbation is given by[34]

$$\frac{\delta n(r,z)}{n_0} = \frac{1}{k_{\rm p}^2}\nabla_\perp^2\left(1 + \frac{a^2}{2}\right)^{1/2}, \quad (65)$$

assuming $\delta n/n_0 \geqslant -1$. With a Gaussian radial profile, $a^2 = a_0^2\exp(-2r^2/r_0^2)$, the laser pulse creates a density profile of

$$\frac{\delta n(r)}{n_0} = -\frac{\Delta n_{\rm c}}{n_0}\frac{a_0^2\exp(-2r^2/r_0^2)}{2\sqrt{1 + a_0^2 e^{-2r^2/r_0^2}/2}}$$
$$\cdot\left[1 - \frac{2r^2}{r_{\rm L}^2} + \frac{a_0^2\exp(-2r^2/r_0^2)}{2(1 + a_0^2 e^{-2r^2/r_0^2}/2)}\frac{r^2}{r_0^2}\right], \quad (66)$$

where $\Delta n_{\rm c} = 1/(\pi r_{\rm e} r_0^2)$ is the critical channel depth for the spot radius r_0 of the guiding laser pulse. Along the axis on $r = 0$, the channel depth is

$$\delta n_0 = |\delta n(0)| = \frac{a_0^2/2}{\sqrt{1 + a_0^2/2}}\Delta n_{\rm c}. \quad (67)$$

The profile of the ponderomotive channel approximates a parabolic density channel as

$$n(r) \simeq n_0 - \delta n_0 + \Delta n_{\rm pond} \frac{r^2}{r_0^2}, \tag{68}$$

where

$$\Delta n_{\rm pond} = \delta n_0 \left[1 - \left(\frac{1 + a_0^2/2}{1 + a_0^2 e^{-2}/2}\right)^{1/2} \cdot \left(3e^{-2} - \frac{a_0^2 e^{-4}/2}{1 + a_0^2 e^{-2}/2}\right)\right]. \tag{69}$$

for $r \leqslant r_0$. Initially assuming a uniform plasma with density n_0 prior to propagating a self-guided laser pulse that creates a ponderomotive channel with the operating plasma density $n_{\rm e}$ given by Eq. (42) in the quasi-linear regime, or by Eq. (61) in the bubble regime, the initial density n_0 is given by

$$n_0 = n_{\rm e}\left(1 - \frac{2a_0^2}{R_{\rm G}^2\sqrt{1 + a_0^2/2}}\right)^{-1}, \tag{70}$$

where $R_{\rm G} \equiv k_{\rm p} r_0$ is the dimensionless matched spot radius for self-guiding, given by

$$R_{\rm G}^2 = k_{p0}^2 r_0^2 = \frac{\ln(1 + a_0^2/2)}{\sqrt{1 + a_0^2/2} - 1 - 2\ln[(\sqrt{1 + a_0^2/2} + 1)/2]}. \tag{71}$$

The channel depth normalized to $n_{\rm e}$ is calculated as

$$\frac{\Delta n_{\rm pond}}{n_{\rm e}} = \frac{2a_0^2}{R_{\rm G}^2\sqrt{1 + a_0^2/2}}\left(1 - \frac{2a_0^2}{R_{\rm G}^2\sqrt{1 + a_0^2/2}}\right)^{-1} \cdot \left[1 - \left(\frac{1 + a_0^2/2}{1 + a_0^2 e^{-2}/2}\right)^{1/2}\left(3e^{-2} - \frac{a_0^2 e^{-4}/2}{1 + a_0^2 e^{-2}/2}\right)\right]. \tag{72}$$

With the channel depth Eq. (72), the matched radius and power of the driving laser pulse propagating through the ponderomotive channel are calculated from Eqs. (27) and (28), respectively, where $a_0 = a_{\rm D}$ and $a_{\rm D}$ is the normalized vector potential of the driving laser pulse. Figure 4 shows an electron density profile $n(r)/n_0$ created by a Gaussian laser pulse with $a_0 = a_{\rm G} = 1.4$ and the parabolic density approximation given by Eq. (68).

The matched spot radius of the guiding laser pulse is given by

$$r_0 = \frac{R_{\rm G}}{k_{\rm p0}} = \frac{\lambda_{\rm L}}{2\pi} R_{\rm G}\sqrt{\frac{n_{\rm c}}{n_0}} \approx 168(\mu{\rm m}) R_{\rm G}\left(\frac{10^{15}\ {\rm cm}^{-3}}{n_0}\right)^{1/2}, \tag{73}$$

and the required matched power of the guiding laser pulse becomes

$$P_{\rm G} = \frac{k_{\rm p0}^2 r_0^2 a_0^2}{32} P_{\rm c} = 0.534({\rm PW}) a_0^2 R_{\rm G}^2 \cdot \left(\frac{1.053\ \mu{\rm m}}{\lambda_{\rm L}}\right)^2 \left(\frac{10^{15}{\rm cm}^{-3}}{n_0}\right). \tag{74}$$

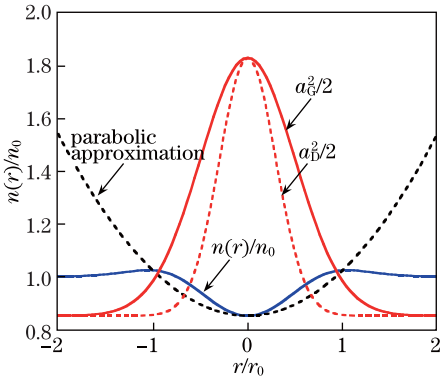

Fig. 4. (Color online) An electron density profile $n(r)/n_0$ (blue solid line) created by a Gaussian laser pulse (red solid line) with $a_{\rm G} = 1.4$ and the parabolic density approximation (black dashed line) given by Eq. (68) are plotted as a function of r/r_0, where r_0 is the spot radius of the guiding laser pulse. A driving laser pulse (red dashed line) with $a_{\rm D} = 1.4$ matched to the channel depth $\Delta n/n_0 = 20\%$ is also plotted.

The pulse duration $\tau_{\rm G}$ is determined from the pump depletion length due to pulse-front erosion $L_{\rm Gpd} \sim c\tau_{\rm G} n_{\rm c}/n_0 \geqslant L_{\rm acc}$, where $L_{\rm acc}$ is the accelerator length, given by Eq. (45) in the quasi-linear regime, or by Eq. (62) in the bubble regime, i.e.,

$$\begin{aligned}\tau_{\rm G} &\geqslant \frac{\kappa_{\rm ch}\lambda_{\rm p0}}{2c}\left(\frac{n_0}{n_{\rm e}}\right)^{3/2} = \frac{\kappa_{\rm ch}\lambda_{\rm L}}{2c}\sqrt{\frac{n_{\rm c}}{n_0}}\left(1 - \frac{2a_0^2}{R_{\rm G}^2\sqrt{1 + a_0^2/2}}\right)^{-3/2} \\ &\approx 1.76({\rm ps})\kappa_{\rm ch}\left(1 - \frac{2a_0^2}{R_{\rm G}^2\sqrt{1 + a_0^2/2}}\right)^{-3/2} \cdot \left(\frac{10^{15}\ {\rm cm}^{-3}}{n_0}\right)^{1/2},\end{aligned} \tag{75}$$

for the quasi-linear regime, or

$$\begin{aligned}\tau_{\rm G} &\geqslant \frac{4\sqrt{a_0}\kappa_{\rm ch}}{ck_{\rm p0}}\left(\frac{n_0}{n_{\rm e}}\right)^{3/2} = \frac{2\kappa_{\rm ch}\sqrt{a_0}\lambda_{\rm L}}{\pi c}\sqrt{\frac{n_{\rm c}}{n_0}}\left(1 - \frac{2a_0^2}{R_{\rm G}^2\sqrt{1 + a_0^2/2}}\right)^{-3/2} \\ &\approx 2.24({\rm ps})\kappa_{\rm ch}\sqrt{a_0}\left(1 - \frac{2a_0^2}{R_{\rm G}^2\sqrt{1 + a_0^2/2}}\right)^{-3/2} \cdot \left(\frac{10^{15}\ {\rm cm}^{-3}}{n_0}\right)^{1/2},\end{aligned} \tag{76}$$

for the bubble regime, respectively. The required pulse energy for the guiding laser pulse is

$$U_{\rm G} = P_{\rm G}\tau_{\rm G} \geqslant 0.94({\rm kJ})\kappa_{\rm ch} a_0^2 R_{\rm G}^2 \cdot \left(1 - \frac{2a_0^2}{R_{\rm G}^2\sqrt{1 + a_0^2/2}}\right)^{-3/2}\left(\frac{1.053\ \mu{\rm m}}{\lambda_{\rm L}}\right)^2$$

$$\cdot \left(\frac{10^{15}\ \mathrm{cm}^{-3}}{n_0}\right)^{3/2}, \tag{77}$$

for the quasi-linear regime, or

$$U_{\mathrm{G}} = P_{\mathrm{G}}\tau_{\mathrm{G}} \geqslant 1.2(\mathrm{kJ})\kappa_{\mathrm{ch}} a_0^{5/2} R_{\mathrm{G}}^2 \cdot \left(1 - \frac{2a_0^2}{R_{\mathrm{G}}^2\sqrt{1+a_0^2/2}}\right)^{-3/2} \left(\frac{1.053\ \mu\mathrm{m}}{\lambda_{\mathrm{L}}}\right)^2 \cdot \left(\frac{10^{15}\mathrm{cm}^{-3}}{n_0}\right)^{3/2}, \tag{78}$$

for the bubble regime, respectively. Figure 5 shows parameters of ponderomotive channel and the guiding laser pulse that can guide a driving laser pulse at the on-axis plasma density $n_{\mathrm{e}} = 7\times10^{15}\ \mathrm{cm}^{-3}$ as a function of normalized vector potential a_0 of the guiding laser pulse.

4. Electron beam dynamics and betatron radiation

Beams that undergo transverse focusing forces $F_\perp = -m_{\mathrm{e}}c^2K^2x$, in plasma waves exhibit the betatron oscillation, where x is the transverse amplitude of betatron oscillation and K is a focusing constant exerted from transverse wakefields. The betatron motion of electrons emits synchrotron radiation that affects energy loss and transverse emittance of the electron beam via the radiation reaction force. The motion of an electron traveling along z-axis in the accelerating force eE_z and the radial force eE_r from the plasma wave evolves according to

$$\frac{\mathrm{d}u_x}{c\mathrm{d}t} = -K^2x + \frac{F_x^{\mathrm{RAD}}}{mc^2}, \frac{\mathrm{d}u_z}{c\mathrm{d}t} = k_{\mathrm{p}}\frac{E_z}{E_0} + \frac{F_z^{\mathrm{RAD}}}{mc^2}, \tag{79}$$

where $\boldsymbol{F}^{\mathrm{RAD}}$ is the radiation reaction force and $\boldsymbol{u} = \boldsymbol{p}/mc$ is the normalized electron momentum. The classical radiation reaction force[43], is given by

$$\frac{\boldsymbol{F}^{\mathrm{rad}}}{mc\tau_{\mathrm{R}}} = \frac{\mathrm{d}}{\mathrm{d}t}\left(\gamma\frac{\mathrm{d}\boldsymbol{u}}{\mathrm{d}t}\right) + \gamma\boldsymbol{u}\left[\left(\frac{\mathrm{d}\gamma}{\mathrm{d}t}\right)^2 - \left(\frac{\mathrm{d}\boldsymbol{u}}{\mathrm{d}t}\right)^2\right], \tag{80}$$

where $\gamma = (1+u^2)^{1/2}$ is the relativistic Lorentz factor of the electron and $\tau_{\mathrm{R}} = 2r_{\mathrm{e}}/3c \simeq 6.26\times10^{-24}$ s. Since the scale length of the radiation reaction, i.e., $c\tau_{\mathrm{R}} = 2r_{\mathrm{e}}/3 \simeq 1.9$ fm, is much smaller than that of the betatron motion, i.e., $\sim \lambda_{\mathrm{p}}\gamma^{1/2}$, assumming that the radiation reaction force is a perturbation and $u_z \gg u_x$, the equations of motion Eq. (79) are approximately written as[44]

$$\frac{\mathrm{d}u_x}{\mathrm{d}t} \simeq -cK^2x - c^2\tau_{\mathrm{R}}K^2u_x(1+K^2\gamma x^2),$$
$$\frac{\mathrm{d}u_z}{\mathrm{d}t} \simeq \omega_{\mathrm{p}}\frac{E_z}{E_0} - c^2\tau_{\mathrm{R}}K^4\gamma^2x^2, \frac{\mathrm{d}x}{\mathrm{d}t} = \frac{cu_x}{\gamma} \simeq c\frac{u_x}{u_z}. \tag{81}$$

Finally, the particle dynamics is obtained from the following coupled equations[29,30,44],

$$\frac{\mathrm{d}^2x}{\mathrm{d}t^2} + \left(\frac{\omega_{\mathrm{p}}}{\gamma}\frac{E_z}{E_0} + \tau_{\mathrm{R}}c^2K^2\right)\frac{\mathrm{d}x}{\mathrm{d}t} + \frac{c^2K^2}{\gamma}x = 0, \tag{82}$$

and

$$\frac{\mathrm{d}\gamma}{\mathrm{d}t} = \omega_{\mathrm{p}}\frac{E_z}{E_0} - \tau_{\mathrm{R}}c^2K^4\gamma^2x^2, \tag{83}$$

where the second damping term proportional to $\tau_{\mathrm{R}}c^2K^2$ results in the linear damping of the betatron motion and the first one induces the nonlinear damping in conjunction with the energy evolution. The radiated power in the classical limit is given by[43]

$$P_{\mathrm{RAD}} = \frac{2e^2\gamma^2}{3c}\left[\left(\frac{\mathrm{d}\boldsymbol{u}}{\mathrm{d}t}\right)^2 - \left(\frac{\mathrm{d}\gamma}{\mathrm{d}t}\right)^2\right] = \frac{2e^2\gamma^2}{3m^2c^3}[|\boldsymbol{F}_{\mathrm{ext}}|^2 - |\mathbf{F}_{\mathrm{ext}}\cdot\boldsymbol{u}/\gamma|^2], \tag{84}$$

using $mc\mathrm{d}\gamma/\mathrm{d}t = \boldsymbol{F}_{\mathrm{ext}}\cdot\boldsymbol{u}/\gamma$, where $\boldsymbol{F}_{\mathrm{ext}}$ is the external force on the electron. As the force is transverse only, i.e., $\boldsymbol{F}_{\mathrm{ext}} = F_\perp\boldsymbol{e}_x$ and for a relativistic electron with $u_x^2 \ll \gamma^2$, the radiated power can be written as[30]

$$P_{\mathrm{RAD}} = \frac{2e^2\gamma^2}{3m^2c^3}F_\perp^2 = \frac{2}{3}ce^2\gamma^2K^4x^2 = mc^4\tau_{\mathrm{R}}K^4\gamma^2x^2, \tag{85}$$

with $F_\perp = -mc^2K^2x$.

Corresponding to Eqs. (82) and (83) describing a single particle dynamics with radiation damping, the envelope equation of the rms beam radius σ_{b} is written as[29,30]

$$\frac{\mathrm{d}^2\sigma_{\mathrm{b}}}{\mathrm{d}z^2} + \left(\frac{k_{\mathrm{p}}}{\gamma}\frac{E_z}{E_0} + \tau_{\mathrm{R}}cK^2\right)\frac{\mathrm{d}\sigma_{\mathrm{b}}}{\mathrm{d}z} + \frac{K^2}{\gamma}\sigma_{\mathrm{b}} - \frac{\varepsilon_0^2}{\sigma_{\mathrm{b}}^3} = 0, \tag{86}$$

$$\frac{\mathrm{d}\gamma}{\mathrm{d}z} = k_{\mathrm{p}}\frac{E_z}{E_0} - 2\tau_{\mathrm{R}}cK^4\gamma^2\sigma_{\mathrm{b}}^2, \tag{87}$$

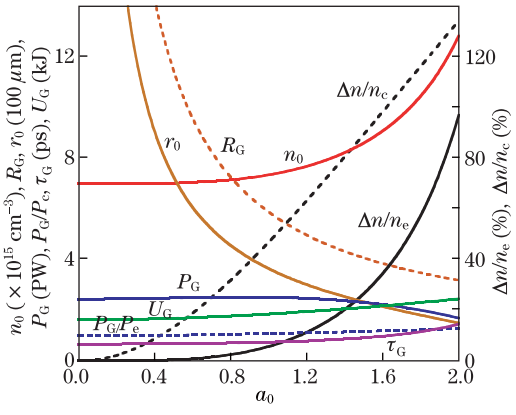

Fig. 5. Parameters of ponderomotive channel and a guiding laser pulse that can guide a driving laser pulse at the on-axis plasma density $n_{\mathrm{e}} = 7\times10^{15}\ \mathrm{cm}^{-3}$ as a function of normalized vector potential a_0 of the guiding laser pulse. Here, n_0 is the initial uniform plasma plasma density in a unit of $10^{15}\ \mathrm{cm}^{-3}$, $R_{\mathrm{G}} = k_{\mathrm{p}}r_0$ is the dimensionless matched spot radius for self-guiding, r_0 is the matched spot radius in a unit of 100 μm, $\Delta n/n_{\mathrm{e}}$ is the ponderomotive channel depth normalized to the on-axis plasma density in percent, $\Delta n/\Delta n_{\mathrm{c}}$ is the ratio of the ponderomotive channel depth to the critical channel depth in percent, P_{G} is the peak power of a guiding laser pulse in a unit of PW, $P_{\mathrm{G}}/P_{\mathrm{c}}$ is the ratio of the peak power to the relativistic self-focusing critical power, τ_{G} is the minimum pulse duration given by Eq. (75) in a unit of ps, and U_{G} is the corresponding pulse energy given by Eq. (77) in a unit of kJ, respectively.

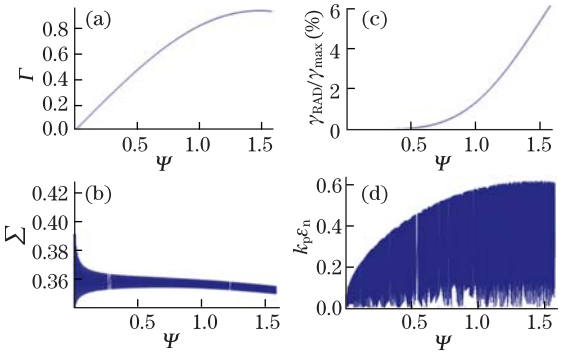

Fig. 6. Numerical solutions of (a) normalized energy $\Gamma = \gamma/(2\chi\gamma_g^2)$, (b) dimensionless beam radius Σ, (c) relative radiative energy loss $\Delta\gamma_{RAD}/(2\chi\gamma_g^2)$, and (d) an estimate of the dimensionless normalized emittance given by Eq. (94) over the dephasing length L_{dp}, i.e., $0 \leqslant \Psi \leqslant \pi/2$, for the quasi-linear regime LPA, $a_0 = 1.4$, $n_e = 7 \times 10^{15}$ cm^{-3}, $\Delta n/n_e = 20\%$, $\chi = E_{z0}/E_0 = 0.745$, $R = k_p r_L = 2.36$, $\kappa_{ch} = 0.913$, $\gamma_0 = 196$ ($W_i = 100$ MeV), and $\Omega_0 = k_p\varepsilon_{n0}/\gamma_0 = 2.12 \times 10^{-4}$.

where $\varepsilon_0 = \varepsilon_{n0}/\gamma_0$ is the initial geometrical emittance at the injection energy γ_0 for the normalized emittance ε_{n0}. The evolution of energy and beam size can be obtained from the solutions of the coupled Eqs. (86) and (87). For simplicity, using the dimensionless variables, $\Sigma \equiv k_p\sigma_b$, $\zeta \equiv k_p z$ and $\Omega_0 \equiv k_p\varepsilon_0$, the coupled equations are rewritten as

$$\frac{d^2\Sigma}{d\zeta^2} + \left(\frac{1}{\gamma}\frac{E_z}{E_0} + \tau_R\omega_p\frac{K^2}{k_p^2}\right)\frac{d\Sigma}{d\zeta} + \frac{1}{\gamma}\frac{K^2}{k_p^2}\Sigma - \frac{\Omega_0^2}{\Sigma^3} = 0, \tag{88}$$

$$\frac{d\gamma}{d\zeta} = \frac{E_z}{E_0} - 2\tau_R\omega_p\frac{K^4}{k_p^4}\gamma^2\Sigma^2. \tag{89}$$

where

$$\tau_R\omega_p = \frac{2}{3}k_p r_e = \frac{4\pi}{3}\frac{r_e}{\lambda_L}\left(\frac{n_c}{n_e}\right)^{-1/2} \approx 1.118 \times 10^{-11}\left(\frac{n_e}{10^{15}\ \text{cm}^{-3}}\right)^{1/2}. \tag{90}$$

4.1 Beam dynamics in the quasi-linear regime

In the quasi-linear regime, the accelerating field E_z/E_0 and the focusing constant K exerted by the wakefields driven by a Gaussian laser pulse with spot radius r_L are expressed by

$$\frac{E_z}{E_0} = \chi\cos\Psi \text{ and } \frac{K^2}{k_p^2} \simeq \frac{4\chi}{R^2}\sin\Psi, \tag{91}$$

where $\Psi(\zeta) \approx \zeta/2\gamma_g^2$ is the dephasing phase of the wakefield,$\chi \equiv E_{z0}/E_0 = 0.38a_0^2$ is the normalized amplitude of the accelerating filed, as shown in Eq. (41), and $R = k_p r_L$ is the dimensionless spot radius of the driving laser pulse. Substituting Eq. (91) into Eqs. (88) and (89), the coupled equations result in

$$\frac{d^2\Sigma}{d\Psi^2} + \left(\frac{\cos\Psi}{\Gamma} + \frac{8\tau_R\omega_p\chi\gamma_g^2}{R^2}\sin\Psi\right)\frac{d\Sigma}{d\Psi} + \frac{8\gamma_g^2}{\Gamma R^2}\Sigma\sin\Psi - \frac{4\gamma_g^4\Omega_0^2}{\Sigma^3} = 0, \tag{92}$$

$$\frac{d\Gamma}{d\Psi} = \cos\Psi - \frac{128\tau_R\omega_p\gamma_g^4\chi^3}{R^4}\Gamma^2\Sigma^2\sin^2\Psi, \tag{93}$$

where $\Gamma \equiv \gamma/(2\chi\gamma_g^2)$ indicates the energy normalized to the maximum energy gain $\Delta\gamma_{max} = 2\chi\gamma_g^2$ as shown in Eq. (39), $R^2 = k_p^2 r_m^2$ and $\gamma_g^2 = \kappa_{ch}\gamma_{g0}^2 = \kappa_{ch}n_c/n_e$ are given by Eqs. (27) and (40), respectively, for laser wakefield acceleration in a plasma channel. The beam energy $\gamma = 2\chi\gamma_g^2\Gamma$ and radius $\sigma_b = \Sigma/k_p$ are obtained from numerically integrating the coupled Eqs. (92) and (93) over $0 \leqslant \Psi \leqslant \pi/2$, provided with the initial conditions $\Sigma_0 = k_p\sigma_{b0}$, $d\Sigma/d\Psi = 0$ and $\Gamma_0 = \gamma_0/(2\chi\gamma_g^2)$ at $\Psi = 0$.

Figure 6 shows the numerical solution of normalized energy Γ and dimensionless beam radius Σ over the dephasing length L_{dp}, i.e., $0 \leqslant \Psi \leqslant \pi/2$, for $a_0 = 1.4$, $n_e = 7 \times 10^{15}$ cm^{-3} and $\Delta n/n_e = 20\%$. It is found that the maximum energy approximately reaches 94 GeV and the equilibrium beam radius becomes $\sigma_{beq} \approx 23$ μm, which decreases as a result of radiative energy loss of ~6% and damps due to betatron radiation in a plasma focusing channel. The normalized emittance corresponding to the equilibrium beam radius is estimated as

$$k_p\varepsilon_n \approx \gamma k_p\varepsilon = \gamma k_p\left|\sigma_b\frac{d\sigma_b}{dz}\right| = \chi\left|\Gamma\Sigma\frac{d\Sigma}{d\Psi}\right|, \tag{94}$$

where ε is the geometrical emittance. The equilibrium normalized emittance is obtained to be $\varepsilon_{neq} \sim 38$ μm from Fig. 6. The evolution of the beam energy W(GeV)

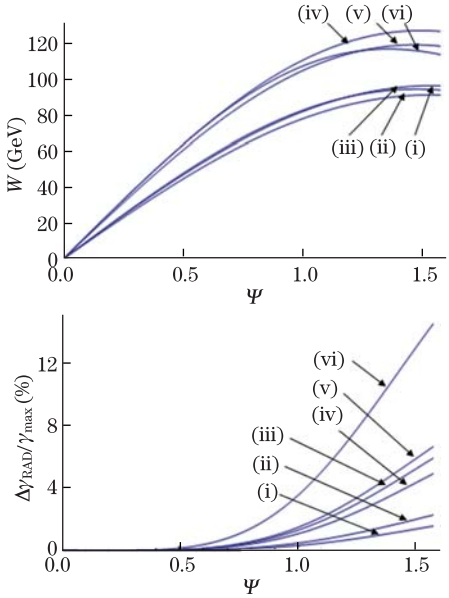

Fig. 7. The evolution of the beam energy W(GeV) and the relative energy loss to the maximum energy gain, $\Delta\gamma_{RAD}/(2\chi\gamma_g^2)$ for the quasi-linear regime LPA. Curves are plotted for the energy $W = 100$ GeV, the channel depth $\Delta n/n_e$ = (i) 5%, (ii) 10%, (iii) 20% case, and the energy $W = 130$ GeV case, the channel depth $\Delta n/n_e$ = (iv) 5% , (v) 10% , (vi) 20% case, respectively.

and the relative energy loss to the maximum energy gain, $\Delta\gamma_{\rm RAD}/(2\chi\gamma_{\rm g}^2)$ are shown in Fig. 7 for the channel depth $\Delta n/n_{\rm e} = 5, 10, 20\%$ and the design energy $W = 100, 130$ GeV cases. As shown in Fig. 7, radiative energy loss increases as the channel depth increases.

4.2 Beam dynamics in the bubble regime

In the bubble or blowout regime[13,14], plasma electrons radially expelled by the radiation pressure of the laser pulse form a sheath with the thickness of the order of the plasma skin depth $c/\omega_{\rm p}$ outside the ion sphere, which is remaining unshielded behind the laser pulse moving at relativistic velocity. As described in Eq. (47), the longitudinal field is given by $|E_z/E_0| = (1/2)\alpha k_{\rm p}\xi$, where $0 \leqslant \xi \leqslant R_{\rm B}$. The transverse fields are composed of the electric fields from the ion sphere $E_{r\rm ion}/E_0 = k_{\rm p}r/2$, the radial plasma current $E_{r\rm EM}/E_0 = -k_{\rm p}r/4$ and the magnetic field from the radial plasma current $B_{\theta\rm EM}/E_0 = -k_{\rm p}r/4$. The total focusing field on a beam electron is $E_r - B_\theta = (1/2)mc^2k_{\rm p}^2r$. Hence, the accelerating field and the focusing constant are given by

$$\frac{E_z}{E_0} = \frac{1}{2}\alpha(k_{\rm p}R_{\rm B} - k_{\rm p}\xi) = \alpha\chi\left(1 - \frac{\zeta}{\zeta_{\rm dp}}\right), \text{ and } \frac{K^2}{k_{\rm p}^2} = \frac{1}{2}, \tag{95}$$

where $\chi = E_{z0}/E_0 = a_0^{1/2}$, $0 \leqslant \zeta \leqslant \zeta_{\rm dp}$ and $\zeta_{\rm dp} = (4/3)\chi\gamma_{\rm g}^2$ is the dimensionless dephasing length for self-guiding case with $\gamma_{\rm g}^2 = \kappa_{\rm self}(n_{\rm c}/n_{\rm e})$, while $\zeta_{\rm dp} = 4\chi\gamma_{\rm g}^2$ is one for the plasma channel case with $\gamma_{\rm g}^2 = \kappa_{\rm ch}(n_{\rm c}/n_{\rm e})$. Using $s = \zeta/\zeta_{\rm dp}$ and Eq. (95), the coupled Eqs. (88) and (89) become

$$\frac{{\rm d}^2\Sigma}{{\rm d}s^2} + 2\left(\frac{1-s}{\Gamma} + \frac{1}{4}\tau_{\rm R}\omega_{\rm p}\zeta_{\rm dp}\right)\frac{{\rm d}\Sigma}{{\rm d}s} + \frac{\zeta_{\rm dp}}{\chi\Gamma}\Sigma - \frac{\zeta_{\rm dp}^2\Omega_0^2}{\Sigma^3} = 0, \tag{96}$$

$$\frac{{\rm d}\Gamma}{{\rm d}s} = 2(1-s) - \frac{1}{4}\tau_{\rm R}\omega_{\rm p}\chi\zeta_{\rm dp}^2\Gamma^2\Sigma^2, \tag{97}$$

where $\Gamma = 2\gamma/(\alpha\chi\zeta_{\rm dp})$ is the dimensionless energy normalized to the maximum energy gain $\Delta\gamma_{\max} = (1/2)\alpha\chi\zeta_{\rm dp} = (2/3)\alpha a_0\gamma_{\rm g}^2$ for the self-guiding case as shown in Eq. (51) or $\Delta\gamma_{\max} = 2\alpha a_0\gamma_{\rm g}^2$ for the plasma channel case as shown in Eq. (59), respectively. For the bubble regime, the evolutions of the beam energy $\gamma = (1/2)\alpha\chi\zeta_{\rm dp}\Gamma$ and radius $\sigma_{\rm b} = \Sigma/k_{\rm p}$ are obtained from numerically integrating the coupled Eqs. (96) and (97) over $0 \leqslant s \leqslant 1$, provided with the initial conditions $\Sigma_0 = k_{\rm p}\sigma_{\rm b0}$, ${\rm d}\Sigma/{\rm d}s = 0$, and $\Gamma_0 = 2\gamma_0/(\alpha\chi\zeta_{\rm dp})$ at $s = 0$.

Figure 8 shows the numerical solution of normalized energy Γ and dimensionless beam radius Σ over the dephasing length $L_{\rm dp}$ for $a_0 = 4$, $n_{\rm e} = 1.87\times10^{16}$ cm^{-3} and $\Delta n/n_{\rm e} = 0\%$ (self-guiding). The maximum energy approximately results in 90 GeV and the equilibrium beam radius becomes $\sigma_{\rm beq} \approx 17$ μm. For the bubble regime case, the normalized emittance corresponding to the equilibrium beam radius is estimated as

$$k_{\rm p}\varepsilon_{\rm n} \approx k_{\rm p}\gamma\left|\sigma_r\frac{{\rm d}\sigma_r}{{\rm d}z}\right| = \frac{\alpha\chi}{2}\Gamma\left|\Sigma\frac{{\rm d}\Sigma}{{\rm d}s}\right|, \tag{98}$$

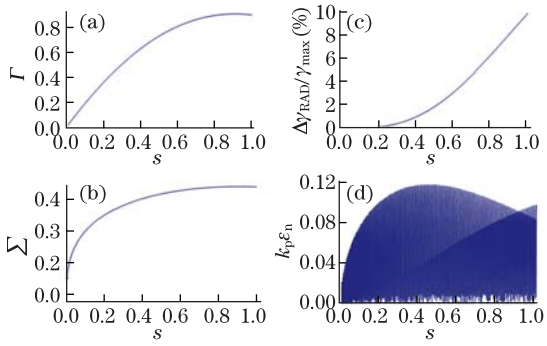

Fig. 8. Numerical solutions of (a) normalized energy $\Gamma = \gamma/(2\alpha\chi^2\gamma_{\rm g}^2/3)$, (b) dimensionless beam radius Σ, (c) relative radiative energy loss $\Delta\gamma_{\rm RAD}/(2\chi^2\gamma_{\rm g}^2/3)$, and (d) an estimate of the dimensionless normalized emittance given by Eq. (98) over the dephasing length $L_{\rm dp}$, i.e., $0 \leqslant s \leqslant 1$, for the self-guided bubble regime LPA, $a_0 = 4$, $n_{\rm e} = 1.87\times10^{16}$ cm^{-3}, $\chi = E_{z0}/E_0 = 2$, $\alpha = 0.9$, $\kappa_{\rm self} = 1.53$, $\gamma_0 = 196$ ($W_{\rm i} = 100$ MeV), and $\Omega_0 = k_{\rm p}\varepsilon_{n0}/\gamma_0 = 3\times10^{-4}$.

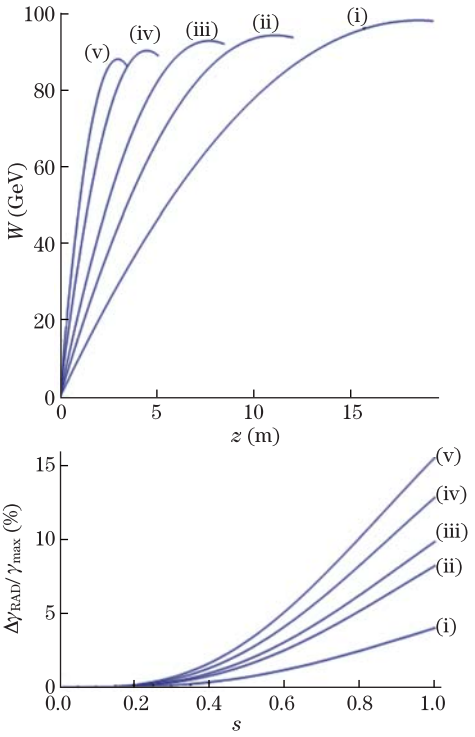

Fig. 9. The evolution of the beam energy W(GeV) as a function of the acceleration length z(m) and the relative energy loss to the maximum energy gain, $\Delta\gamma_{\rm RAD}/(2\alpha a_0\gamma_{\rm g}^2/3)$ for the self-guiding bubble regime LPA. Curves are plotted for (i) $a_0 = 2$, $n_{\rm e} = 7.3\times10^{15}$ cm^{-3}, (ii) $a_0 = 3$, $n_{\rm e} = 1.2\times10^{16}$ cm^{-3}, (iii) $a_0 = 4$, $n_{\rm e} = 1.9\times10^{16}$ cm^{-3}, (iv) $a_0 = 6$, $n_{\rm e} = 3.5\times10^{16}$ cm^{-3}, and (v) $a_0 = 8$, $n_{\rm e} = 5.5\times10^{16}$ cm^{-3}, respectively, assuming $\alpha = 0.9$.

which gives the equilibrium normalized emittance $\varepsilon_{\rm neq} \sim 4.7$ μm, assuming $\alpha = 0.9$. The evolution of the beam energy W(GeV) and the relative energy loss to the maximum energy gain, $\Delta\gamma_{\rm RAD}/(2\alpha a_0\gamma_{\rm g}^2/3)$ are shown in Fig. 9 for $a_0 = 2, 3, 4, 6, 8$. As shown in Fig. 9, the accelerator length decreases with a_0, while radiative energy loss increases with a_0.

4.3 Radiative energy loss due to betatron radiation

Assuming that the electron beam has an equilibrium radius defined by

$$\sigma_{\rm eq}^2 = \frac{\varepsilon_0}{K}\gamma^{1/2} \approx \text{const.}, \tag{99}$$

the radiative energy loss due to betatron radiation can be estimated from

$$\Delta\gamma_{\rm RAD} \approx 2\rho\int_{\gamma_0}^{\gamma_{\rm M}} {\rm d}\gamma(\gamma^2 + 2\rho\gamma^4), \tag{100}$$

where $\gamma_{\rm M}$ is the electron energy without radiation and a coefficient of radiative loss

$$\rho \equiv \tau_{\rm R}\omega_{\rm p}k_{\rm p}^2\sigma_{\rm eq}^2\left(\frac{E_z}{E_0}\right)^{-1}\left(\frac{K}{k_{\rm p}}\right)^4 \ll 1, \tag{101}$$

is assumed. Taking into account $\gamma_0 \ll \gamma_{\rm M}$ and $\gamma_{\rm M} = \gamma - \Delta\gamma_{\rm RAD}$, the relative radiative energy loss becomes

$$\begin{aligned}\frac{\Delta\gamma_{\rm RAD}}{\gamma} &\approx \frac{2}{3}\rho\gamma^2\frac{1+(6/5)\rho\gamma^2}{1-2\rho\gamma^2(1+2\rho\gamma^2)} \\ &= \frac{2}{3}\rho_0\gamma^{5/2}\frac{1+(6/5)\rho_0\gamma^{5/2}}{1-2\rho_0\gamma^{5/2}(1+2\rho_0\gamma^{5/2})}.\end{aligned} \tag{102}$$

where with the initial normalized emittance $\varepsilon_{\rm n0}$

$$\begin{aligned}\rho_0 &\equiv \tau_{\rm R}\omega_{\rm p}\Omega_0\left(\frac{E_z}{E_0}\right)^{-1}\left(\frac{K}{k_{\rm p}}\right)^3 \\ &= \frac{8}{3}\pi r_{\rm e}^2 n_{\rm e}\frac{\varepsilon_{\rm n0}}{\gamma_0}\left(\frac{E_z}{E_0}\right)^{-1}\left(\frac{K}{k_{\rm p}}\right)^3 \\ &= 66.5\times10^{-15}\gamma_0^{-1}\left(\frac{\varepsilon_{\rm n0}}{1\ \mu{\rm m}}\right)\left(\frac{n_{\rm e}}{10^{15}\ {\rm cm}^{-3}}\right) \\ &\cdot\left(\frac{E_z}{E_0}\right)^{-1}\left(\frac{K}{k_{\rm p}}\right)^3.\end{aligned} \tag{103}$$

In the bubble regime wakefields driven by a_0, the relative radiation loss is approximately given by

$$\begin{aligned}\frac{\Delta\gamma_{\rm RAD}}{\gamma} &\approx 0.136\times10^{-2}a_0^{-1/2}\left(\frac{\varepsilon_{\rm n0}}{1\ \mu{\rm m}}\right)\left(\frac{n_{\rm e}}{10^{15}\ {\rm cm}^{-3}}\right) \\ &\cdot\left(\frac{W}{100\ {\rm GeV}}\right)^{5/2}\left(\frac{W_{\rm i}}{100\ {\rm MeV}}\right)^{-1},\end{aligned} \tag{104}$$

where $W_{\rm i}$ is the injection energy. As an example, for $a_0 = 4$, $n_{\rm e} = 1.4\times10^{16}$ cm^{-3} and $W_{\rm i} = 100$ MeV, the relative energy loss at 100 GeV is approximately$\Delta\gamma_{\rm RAD}/\gamma \approx 1.0\times10^{-2}(\varepsilon_{\rm n0}/1\ \mu{\rm m})$.

5. Discussions and conclusions

We have considered the possible designs of LPAs for reaching 100 GeV and 130 GeV, utilizing a large-scale laser such as a 500-fs, 3.5-kJ pulse delivered from the PETAL laser and the experimental facility at LMJ. A goal of this experiment is to demonstrate acceleration of 100-GeV-level electron beams with high-quality properties, such as a 1% energy spread and a 1π mm-mrad normalized emittance. To accomplish the goal and satisfy the guideline on the LPA scaling and laser facility, we propose three LPA options: the channel-guided LPA operated in the quasi-linear regime, the self-guided LPA operated in the nonlinear bubble (or blowout) regime, and the ponderomotive channel-guided LPA, which is a hybrid concept composed of a self-guided channel creator pulse with a long duration and a large spot radius, followed by the driving laser pulse for the quasi-linear regime LPA with a shorter duration and a smaller radius than the creator pulse. As an electron injector in the front end of large-scale LPAs that require the high-quality beam injection with charge of ∼100 pC and low emittance, the ionization-induced injection is suitable for controlling trapped charge and energy spread, and keeping the transverse beam emittance small, which turns out to significant energy loss due to betatron radiation from e-beams at high energies. The detailed parameters on requirements of the laser pulse and plasma are listed in Table 1.

Plasma waveguides for guiding ultraintense short laser pulses in plasmas are produced by a number of methods, including laser-induced hydrodynamic expansion[45−47], pulsed discharges of an ablative capillary[4,5,48,49] or a gas-filled capillary[50,51]. However, the length of such a plasma channel has been limited to less than 10 cm and the plasma density has been created for $n_0 \geqslant 10^{17}$ cm^{-3}. For a low-density ($n_0 \sim 10^{14} - 10^{17}$ cm^{-3}) large-scale (∼1–10 m) plasma waveguide, proposed is a radio frequency (RF) discharge plasma technique that creates hollow electron density profiles by means of a quadrupole rod antenna and helicon wave antennas. Possible advantages of the RF discharge technique are stability and a meter-scale length in addition to a long lifetime, high production efficiency and high repetition rate over those of laser-induced channels and capillary discharges. One of disadvantages that have not been resolved includes the

Table 1. Parameters for 100-GeV Level Laser Plasma Acceleration

Option	A	B	C	D	E	
W(GeV)	100	133	100	100		100
$n_{\rm e}(\times10^{15}\ {\rm cm}^{-3})$	7	7	12	35	8.2	7
$\Delta n/n_{\rm e}(\%)$	20	20	0	0	0	20
$L_{\rm dp}$(m)	26	27	12	5.1	45	26
a_0	1.4	1.6	3	6	1.4	1.4
$r_{\rm m}(\mu{\rm m})$	180	168	110	41	253	180
$k_{\rm p}r_{\rm m}$	2.83	2.63	2.3	1.5	4.3	2.83
P(PW)	1.21	1.37	2.1	1.2	2.4	1.21
$P/P_{\rm c}$	0.49	0.55	1.5	2.4	1.1	0.49
$\tau_{\rm L}$(fs)	500	500	500	500	1 200	500
U(kJ)	0.61	0.69	1.1	0.6	2.6	0.61
$\sigma_{\rm b}(\mu{\rm m})$	23	21	19	14		23
$k_{\rm p}\sigma_b$	0.36	0.34	0.40	0.48		0.36
$\Delta\gamma_{\rm RAD}/\gamma_{\rm max}(\%)$	6	15	8	13		6

use of high neutral gas pressure for producing high density plasma, where neutral gas remnants may change the density profile due to further ionization at the moment guided high-intensity laser pulses propagate in plasma channels. To guide ultraintense laser pulses, plasma channels must be produced in fully ionized gases with low atomic number Z such as hydrogen or helium. However, at present none of them are available for the use of large-scale LPAs at the low plasma density region over the 30-m length, although researches and developments of such plasma waveguides are vibrantly carried out.

In conclusion, possible experiments on large-scale laser plasma acceleration are proposed, aiming at the 100-GeV level electron beam acceleration by the use of large-scale lasers such as the PETAL at CEA-LMJ delivering 3.5-kJ, 500-fs pulses. The experiment explores laser-plasma acceleration physics including the long propagation of relativistic laser pulses and electron beam dynamics associated with strong betatron radiation at the 100-GeV level as well as feasibility of laser-based high energy particle physics.

The authors would like to thank G. Mourou and T. Tajima at IZEST for their fruitful suggestions and discussions. The work was supported by the National Natural Science Foundation of China (Nos. 10834008, 10974214, 60921004, and 51175324) and the National "973" Program of China (Nos. 2011CB808104, 2011CB808100, and 2010CB923203). K. Nakajima is supported by Chinese Academy of Sciences Visiting Professorship for Senior International Scientists (No. 2010T2G02).

References

1. T. Tajima and J. M. Dawson, Phys. Rev. Lett. **43,** 267 (1979).
2. W. P. Leemans, B. Nagler, A. J. Gonsalves, C. Toth, K. Nakamura, C. G. R. Geddes, E. Esarey, C. B. Schroeder, and S. M. Hooker, Nat. Phys. **2,** 696 (2006).
3. C. E. Clayton, J. E. Ralph, F. Albert, R. A. Fonseca, S. H. Glenzer, C. Joshi, W. Lu, K. A. Marsh, S. F. Martins, W. B. Mori, A. Pak, F. S. Tsung, B. B. Pollock, J. S. Ross, L. O. Silva, and D. H. Froula, Phys. Rev. Lett. **105,** 105003 (2010).
4. H. Lu, M. Liu, W. Wang, C. Wang, J. Liu, A. Deng, J. Xu, C. Xia, W. Li, H. Zhang, X. Lu, C. Wang, J. Wang, X. Liang, Y. Leng, B. Shen, K. Nakajima, R. Li, and Z. Xu, Appl. Phys. Lett. **99,** 091502 (2011).
5. T. Kameshima, W. Hong, K. Sugiyama, X. Wen, Y. Wu, C. Tang, Q. Zhu, Y. Gu, B. Zhang, H. Peng, S.-i. Kurokawa, L. Chen, T. Tajima, T. Kumita, and K. Nakajima, Appl. Phys. Express **1,** 066001 (2008).
6. S. Karsch, J. Osterhoff, A. Popp, T. P. Rowlands-Rees, Z. Major, M. Fuchs, B. Marx, R. Hörlein, K. Schmid, L. Veisz, S. Becker, U. Schramm, B. Hidding, G. Pretzler, D. Habs, F. Grüner, F. Krausz, and S. M. Hooker, New J. Phys. **9,** 415 (2007).
7. O. Lundh, J. Lim, C. Rechatin, L. Ammoura, A. Ben-Ismail, X. Davoine, G. Gallot, J. P. Goddet, E. Lefebvre, V. Malka, and J. Faure, Nat. Phys. **7,** 219 (2011).
8. J. Osterhoff, A. Popp, Z. Major, B. Marx, T. P. Rowlands-Rees, M. Fuchs, M. Geissler, R. Horlein, B. Hidding, S. Becker, E. A. Peralta, U. Schramm, F. Gruner, D. Habs, F. Krausz, S. M. Hooker, and S. Karsch, Phys. Rev. Lett. **101,** 085002 (2008).
9. N. A. M. Hafz, T. M. Jeong, I. W. Choi, S. K. Lee, K. H. Pae, V. V. Kulagin, J. H. Sung, T. J. Yu, K.-H. Hong, T. Hosokai, J. R. Cary, D.-K. Ko, and J. Lee, Nat. Photon. **2,** 571 (2008).
10. S. P. D. Mangles, C. D. Murphy, Z. Najmudin, A. G. R. Thomas, J. L. Collier, A. E. Dangor, E. J. Divall, P. S. Foster, J. G. Gallacher, C. J. Hooker, D. A. Jaroszynski, A. J. Langley, W. B. Mori, P. A. Norreys, F. S. Tsung, R. Viskup, B. R. Walton, and K. Krushelnick, Nature **431,** 535 (2004).
11. C. G. R. Geddes, C. Toth, J. van Tilborg, E. Esarey, C. B. Schroeder, D. Bruhwiler, C. Nieter, J. Cary, and W. P. Leemans, Nature **431,** 538 (2004).
12. J. Faure, Y. Glinec, A. Pukhov, S. Kiselev, S. Gordienko, E. Lefebvre, J. P. Rousseau, F. Burgy, and V. Malka, Nature **431,** 541 (2004).
13. I. Kostyukov, A. Pukhov, and S. Kiselev, Phys. Plasmas **11,** 5256 (2004).
14. W. Lu, C. Huang, M. Zhou, W. B. Mori, and T. Katsouleas, Phys. Rev. Lett. **96,** 165002 (2006).
15. J. Faure, C. Rechatin, A. Norlin, A. Lifschitz, Y. Glinec, and V. Malka, Nature **444,** 737 (2006).
16. H. Kotaki, I. Daito, M. Kando, Y. Hayashi, K. Kawase, T. Kameshima, Y. Fukuda, T. Homma, J. Ma, L. M. Chen, T. Z. Esirkepov, A. S. Pirozhkov, J. K. Koga, A. Faenov, T. Pikuz, H. Kiriyama, H. Okada, T. Shimomura, Y. Nakai, M. Tanoue, H. Sasao, D. Wakai, H. Matsuura, S. Kondo, S. Kanazawa, A. Sugiyama, H. Daido, and S. V. Bulanov, Phys. Rev. Lett. **103,** 194803 (2009).
17. K. Schmid, A. Buck, C. M. S. Sears, J. M. Mikhailova, R. Tautz, D. Herrmann, M. Geissler, F. Krausz, and L. Veisz, Phys. Rev. ST Accel. Beams **13** (2010).
18. A. J. Gonsalves, K. Nakamura, C. Lin, D. Panasenko, S. Shiraishi, T. Sokollik, C. Benedetti, C. B. Schroeder, C. G. R. Geddes, J. van Tilborg, J. Osterhoff, E. Esarey, C. Toth, and W. P. Leemans, Nat. Phys. **7,** 862 (2011).
19. A. Pak, K. A. Marsh, S. F. Martins, W. Lu, W. B. Mori, and C. Joshi, Phys. Rev. Lett. **104,** 025003 (2010).
20. C. McGuffey, A. G. R. Thomas, W. Schumaker, T. Matsuoka, V. Chvykov, F. J. Dollar, G. Kalintchenko, V. Yanovsky, A. Maksimchuk, K. Krushelnick, V. Y. Bychenkov, I. V. Glazyrin, and A. V. Karpeev, Phys. Rev. Lett. **104,** 025004 (2010).
21. C. Xia, J. Liu, W. Wang, H. Lu, W. Cheng, A. Deng, W. Li, H. Zhang, X. Liang, Y. Leng, X. Lu, C. Wang, J. Wang, K. Nakajima, R. Li, and Z. Xu, Phys. Plasmas **18,** 113101 (2011).
22. J. S. Liu, C. Q. Xia, W. T. Wang, H. Y. Lu, C. Wang, A. H. Deng, W. T. Li, H. Zhang, X. Y. Liang, Y. X. Leng, X. M. Lu, C. Wang, J. Z. Wang, K. Nakajima, R. X. Li, and Z. Z. Xu, Phys. Rev. Lett. **107,** 035001 (2011).
23. B. B. Pollock, C. E. Clayton, J. E. Ralph, F. Albert, A. Davidson, L. Divol, C. Filip, S. H. Glenzer, K. Herpoldt, W. Lu, K. A. Marsh, J. Meinecke, W. B. Mori, A. Pak, T. C. Rensink, J. S. Ross, J. Shaw, G. R. Tynan, C. Joshi, and D. H. Froula, Phys. Rev. Lett. **107,** 045001 (2011).
24. S. F. Martins, R. A. Fonseca, W. Lu, W. B. Mori, and L. O. Silva, Nat. Phys. **6,** 311 (2010).
25. C. B. Schroeder, E. Esarey, C. G. R. Geddes, C. Benedetti, and W. P. Leemans, Phys. Rev. ST Accel. Beams **13,** 101301 (2010).
26. K. Nakajima, A. Deng, X. Zhang, B. Shen, J. Liu, R. Li, Z. Xu, T. Ostermayr, S. Petrovics, C. Klier, K. Iqbal, H. Ruhl, and T. Tajima, Phys. Rev. ST Accel. Beams **14,** 091301 (2011).

27. N. Blanchot, E. Bar, G. Behar, C. Bellet, D. Bigourd, F. Boubault, C. Chappuis, H. Coïc, C. Damiens-Dupont, O. Flour, O. Hartmann, L. Hilsz, E. Hugonnot, E. Lavastre, J. Luce, E. Mazataud, J. Neauport, S. Noailles, B. Remy, F. Sautarel, M. Sautet, and C. Rouyer, Opt. Express **18,** 10088 (2010).
28. T. Tajima, M. Kando, and M. Teshima, Prog. Theor. Phys. **125,** 617 (2011).
29. A. Deng, K. Nakajima, X. Zhang, H. Lu, B. Shen, J. Liu, R. Li, and Z. Xu, Laser Part. Beams **30,** 281 (2012).
30. A. Deng, K. Nakajima, J. Liu, B. Shen, X. Zhang, Y. Yu, W. Li, R. Li, and Z. Xu, Phys. Rev. ST Accel. Beams **15,** 081303 (2012).
31. X. M. Wang, S. A. Yi, R. Zgadzaj, N. Fazel, W. Henderson, Y.-Y. Chang, R. Korzekwa, V. Khudik, G. Shvets, H.-E. Tsai, C.-H. Pai, Z. Li, E. Gaul, M. Martinez, H. Quevedo, T. Borger, M. Spinks, M. Donovan, A. Bernstein, G. Dyer, T. Ditmire, and M. Downer, "Physics of electron acceleration beyond 1 GeV at the Texas Petawatt Laser," talk at the 15th Advanced Accelerator Concepts Workshop (2012).
32. B. Hafizi, A. Ting, R. F. Hubbard, P. Sprangle, and J. R. Penano, Phys. Plasmas **10,** 1483 (2003).
33. C. B. Schroeder, C. Benedetti, E. Esarey, J. van Tilborg, and W. P. Leemans, Phys. Plasmas **18,** 083103 (2011).
34. B. Hafizi, A. Ting, P. Sprangle, and R. F. Hubbard, Phys. Rev. E **62,** 4120 (2000).
35. E. Esarey and W. P. Leemans, Phys. Rev. E **59,** 1082 (1999).
36. P. Sprangle, A. Ting, and C. M. Tang, Phys. Rev. A **36,** 2773 (1987).
37. P. Sprangle, B. Hafizi, and J. R. Penano, Phys. Rev. E **61,** 4381 (2000).
38. M. Liu, B. Zhou, Y. Yi, X. Liu, and L. Tang, Phys. Plasmas **14,** 103104 (2007).
39. M. Liu, R. Li, Z. Xu, and C.-J. Kim, Phys. Lett. A **373,** 363 (2009).
40. M. Chen, E. Esarey, C. B. Schroeder, C. G. R. Geddes, and W. P. Leemans, Phys. Plasmas **19,** 033101 (2012).
41. C. Chiu, S. Cheshkov, and T. Tajima, Phys. Rev. ST Accel. Beams **3,** 101301 (2000).
42. W. Lu, M. Tzoufras, C. Joshi, F. S. Tsung, W. B. Mori, J. Vieira, R. A. Fonseca, and L. O. Silva, Phys. Rev. ST Accel. Beams **10,** 061301 (2007).
43. J. D. Jackson, Classical Electrodynamics, 3rd Edition (John Wiley & Sons, New York, 1999).
44. P. Michel, C. B. Schroeder, B. A. Shadwick, E. Esarey, and W. P. Leemans, Phys. Rev. E **74,** 026501 (2006).
45. C. G. Durfee, III and H. M. Milchberg, Phys. Rev. Lett. **71,** 2409 (1993).
46. P. Volfbeyn, E. Esarey, and W. P. Leemans, Phys. Plasmas **6,** 2269 (1999).
47. Y. F. Xiao, H. H. Chu, H. E. Tsai, C. H. Lee, J. Y. Lin, J. Wang, and S. Y. Chen, Phys. Plasmas **11,** L21 (2004).
48. Y. Ehrlich, C. Cohen, A. Zigler, J. Krall, P. Sprangle, and E. Esarey, Phys. Rev. Lett. **77,** 4186 (1996).
49. M. Liu, A. Deng, J. Liu, R. Li, J. Xu, C. Xia, C. Wang, B. Shen, Z. Xu, and K. Nakajima, Rev. Sci. Instrum. **81,** 036107 (2010).
50. T. Hosokai, M. Kando, H. Dewa, H. Kotaki, S. Kondo, N. Hasegawa, K. Nakajima, and K. Horioka, Opt. Lett. **25,** 10 (2000).
51. S. M. Hooker, D. J. Spence, and R. A. Smith, J. Opt. Soc. Am. B **17,** 90 (2000).